Power Management and Control for Solar-Wind-Diesel Stand-alone Hybrid Energy Systems

By

Md. Aminul Islam

A Thesis Submitted to Saint Mary's University, Halifax, Nova Scotia

in Partial Fulfillment of the Requirements for

the Degree of Master of Science in Applied Science

July 4, 2014, Halifax, Nova Scotia

Approved:	Dr. Adel Merabet Co-Supervisor Division of Engineering
Approved:	Dr. Rachid Beguenane Co-Supervisor ECE, Royal Military College
Approved:	Dr. M.E. El-Hawary External Examiner Faculty of Engineering Dalhousie University
Approved:	Dr. Vlodek Tarnawski Supervisory Committee Member Division of Engineering
Approved:	Dr. Kai Ylijoki Chair of Defense Graduate Studies Representative
Date:	July 4, 2014

Power Management and Control Systems for Solar-Wind-Diesel Stand-alone Hybrid Energy Systems

by Md. Aminul Islam

Abstract

A simulation based research on developing a power management and control system for stand-alone solar-wind-diesel hybrid energy systems is presented in this dissertation. The simulation model of stand-alone system is developed from mathematical models of solar photovoltaic system, wind turbines and diesel generators. A multi-variable control system is developed and implemented into the simulation models in order to achieve optimum performance. The model of solar photovoltaic energy conversion system is constructed with maximum power point tracking control to extract maximum power from the solar photovoltaic system. An improved control system is developed for wind energy conversion system to optimize the operation of wind turbine through speed regulation and maximum power point tracking control. In addition, a governor control system is developed for the diesel generation system. The frequency regulation system consist conventional phase locked loop system and a voltage regulator in order to regulate the load voltage. A power management strategy is introduced to share the generated power and to improve the power quality where priority is given to the wind energy conversion system. The power management algorithm controls the sharing of generated power and optimizes the hybrid operation. The complete model of stand-alone solar-wind-diesel hybrid energy system is simulated in Matlab®/Simulink® interface. Results obtained from the simulation are presented to validate the control algorithms developed in this work.

July 4th, 2014

Acknowledgement

I would like to express the deepest appreciation to all who helped me to successfully complete my project. First of all, I would like to thank Saint Mary's University for providing me the opportunity to pursue the MSc in Applied Science program with funding and Research Fellowship. I am grateful to my supervisor, Dr. Adel Merabet, for his continuous support. Without his guidance and valuable help this thesis would not be successful. I am thankful for the support provided by my co-supervisor, Dr. Rachid Beguenane, from the Royal Military College of Canada, Kingston, Ontario.

In addition, I would like to thank my supervisory committee member, Dr. Vlodek Tarnawski, and the external examiner, Dr. M. E. El-Hawary, for their valuable comments and suggestions provided for my thesis. Without their guidance and feedback, this work could not have been a success. I am grateful to Dr. Hussein Ibrahim and TechnoCentre Éolien for the technical visit to the site of the micro-grid project in Gaspé, Quebec. I would also like to thank the entire research group of Laboratory of Control Systems and Mechatronics (LCSM), Division of Engineering at Saint Mary's University for their support and help. I also thank all the university officials who helped me in many ways throughout my program of study.

Finally, I express my gratitude to my parents for their constant support and encouragement throughout my years of study. This accomplishment would not have been possible without them.

July 4th, 2014

Table of Contents

List of Figures

List of Tables

Nomenclature

Solar Photovoltaic Cell

B	Solar irradiance
I	Load current
I_{PH}	Photocurrent
I_{RS}	Diode reverse saturation current
I_S	Diode saturation current
I_{SC}	Short circuit current
K	Boltzmann's constant
K_i	Temperature coefficient of short circuit current
N	Diode ideality factor
P	Cell generated power
PV	Photovoltaic
q	Electron charge
R_S	Series resistance
R_{SH}	Shunt resistance
T	Cell temperature
T_{ref}	Reference temperature
V	Cell terminal voltage
V_{OC}	Open circuit voltage
V_t	Thermal voltage

MPPT for PVECS

I	Operating load current
U	Operating load voltage
U_{max}	Maximum voltage
U_{ref}	Reference voltage

Wind Energy Conversion

P_{air}	Power in the airflow
ρ	Air density
A	Swept area of rotor
v	Wind speed
P_M	Mechanical power
C_p	Power coefficient
λ	Tip-speed ratio
ω	Rotational speed of rotor
R	Radius of tip of rotor

Permanent Magnet Synchronous Generator

L_d	d-axis inductance
L_q	q-axis inductance
R	Resistance of the stator windings
i_d	d-axis current
i_q	q-axis current
v_d	d-axis voltage
v_q	q-axis voltage

ω_r	Angular velocity of the rotor
φ	Rotor flux
p	Number of poles
T_e	Electromagnetic torque

MPPT for WECS

α	Positive gain
k	Speed factor
P_m	Mechanical power produce by the wind turbine
ω_r	Turbine rotor shaft speed
ω_{ref}	Speed reference

Synchronous Generator

i_{kd}	Damper winding current
i_{fd}	Field current
φ_{mq}	q-axis mutual flux
φ_{md}	d-axis mutual flux
V_q	q-axis stator voltage
V_d	d-axis stator voltage
ω_q	Mechanical rotor speed
T_e	Electromagnetic torque
T_m	Mechanical torque
H	Inertia constant
K_d	Damping factor
ω_0	Speed of operation

R_S	Stator resistance
L_{ls}	Stator leakage inductance
L_{md}	d-axis magnetizing inductance
L_{mq}	q-axis magnetizing inductance
R_f	Field resistance
L'_{fd}	Field leakage inductance
R'_{kd}	d-axis damper resistance
R'_{kq}	q-axis damper resistance
L'_{lkd}	d-axis damper leakage inductance
L'_{lkq1}	q-axis damper leakage inductance
L'_{lkq2}	q-axis damper leakage inductance
J	Inertial coefficient
P	Number of pole pairs
T_f	Friction torque
φ'_{fd}	Field winding d-axis flux
φ'_{kd}	Damper winding d-axis flux
φ'_{kq1}	Damper winding q-axis flux
φ'_{kq2}	Damper winding q-axis flux

Acronyms and Abbreviations

AC	Alternating Current
DC	Direct Current
DE	Diesel Engine
DECS	Diesel Energy Conversion System
GTO	Gate Turn-off
HES	Hybrid Energy Systems
HIL	Hardware-in-the-Loop
IGBT	Insulated Gate Bipolar Transistor
MOSFET	Metal Oxide Semiconductor Field Effect Transistor
MPP	Maximum Power Point
MPPT	Maximum Power Point Tracking
PD	Proportional-Derivative
PI	Proportional-Integral
PID	Proportional-Integral-Derivative
PLL	Phase Locked Loop
PMSG	Permanent Magnet Synchronous Generator
PMSM	Permanent Magnet Synchronous Machine
P&O	Perturb & Observe
PV	Photovoltaic
PVECS	Photovoltaic Energy Conversion System
PWM	Pulse Width Modulation

STC	Standard Test Condition
SWDHES	Solar-Wind-Diesel Hybrid Energy System
VSC	Voltage Source Converter
WECS	Wind Energy Conversion System

Chapter 1

1 Introduction

Electrical power systems are facing many challenges in development and expansion. These are no longer limited in technical, economic, or financial in nature but are environmental and social. Climate change and sustainable development are major challenges of the 21st century, with extraordinary implications for energy and environmental security [1]. The utilization of traditional energy sources such as natural gas, coal and oil causes the increase of electrical energy generation cost besides their pollutant effects to environment [2]. A rapid growth of the energy demand is affecting the environment and leaving a long lasting harmful effect on the environment. Renewable energy resources like wind energy, solar PV and tidal energy have the potential to overcome these difficulties.

For different regions and locations, climatic conditions including solar irradiance, temperature and wind speed are continuously changing. It may cause the instability shortcoming for electrical power generation from solar photovoltaic and wind turbines. In order to efficiently and economically utilize the renewable energy resources the concept of Hybrid Energy Systems (HES) has been proposed.

This work focuses on the development of power management systems, control systems for solar-wind-diesel hybrid energy system, test and validate the algorithms in simulation

interface. Mathematical modeling is required to develop and simulate the model of solar photovoltaic, wind and diesel energy conversion system.

In this chapter, a detail background of the system approach and feasibility of hybrid operation is discussed. The basic principles of solar photovoltaic, wind energy conversion systems and maximum power point tracking (MPPT) algorithm is also introduced to give an overview of the major system components.

1.1 Current Status and Background

A modern power network is one that takes advantage of leading technologies to improve power grid efficiency, reliability and flexibility. A number of technical, economical and societal factors are coming together to make microgrids the biggest driving change in the electric power infrastructure on the horizon. The cost of distributed generation is continuing to drop and is competitive with grid-supplied power in many regions. For example, photovoltaic (PV) panels and inverters continue to decline in cost and clean natural gas fired and diesel generation is inexpensive because of very low gas prices [3]. The significance of integrating renewable energy sources are now considered as potential solution for a sustainable future.

The stand-alone hybrid solar-wind power generation system is recognized as a viable alternative to grid supply or to conventional fossil fuel based remote area power supplies all over the world. There are approximately 292 off-grid Canadian remote communities with a total population of approximately 194,281 people (2006 Statistics Canada Census); they have significant wind energy potentials [4]. The annual demand is approximately

1,477,415 MWh/yr where fossil fuel generation type is mostly diesel. As the operation of diesel generators are highly expensive and contribute in carbon emission an alternative solution is required to minimize the diesel consumption. In the period of 2008-2011 the annual growth rate of solar photovoltaic power was 147.3% in Canada [5]. At the same time wind power generation has gained popularity and is estimated to produce 12% of the world's electricity by 2020 [6]. Consequently, the idea of hybrid operation is gaining attention among the researchers in electrical power industry.

TechnoCentre Éolien (TCÉ) has developed an infrastructure of hybrid renewable energy operation in Gaspé, Quebec. The main purpose of this project is to study the potential applications and operation of the stand-alone hybrid energy system. The current infrastructure consists of one wind power plant, one diesel power plant, one compressed air storage unit, one motor-generator electric drive (MGSet), one battery bench, one heat exchanger, one resistive load, secondary loads and one remote monitoring system [7]. The proposed design of TechnoCentre Éolien micro-grid is shown in fig. 1.

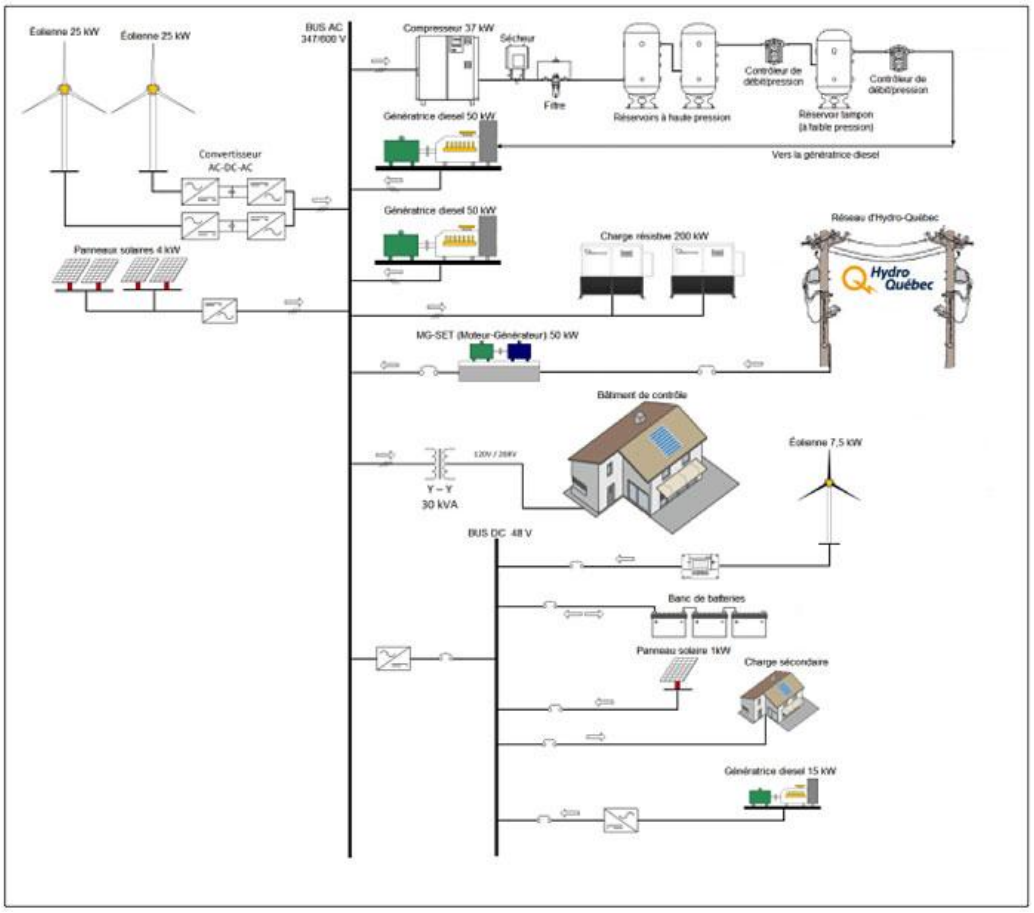

Figure 1 Proposed design of the micro-grid project by TCÉ [7]

A provision to implement solar photovoltaic system is also included in this project. A part of the TCÉ system is taken into consideration in this simulation based research. This research was being conducted according to the project specification in Quebec so the power management strategy and control algorithms are applied in simulation to study the hybrid operation of solar-wind-diesel energy conversion system. TechnoCentre Éolien may apply the configuration and algorithm developed in this work.

1.2 Literature Review

Literature review on hybrid energy system is very extensive. However, a brief literature review is done to facilitate the work conducted in this study. Since the study includes the operation of hybrid energy system consisting solar, wind and diesel energy systems, following topics are considered in developing the simulation model:

i. Feasibility studies
ii. Wind energy conversion systems
iii. Solar photovoltaic energy conversion systems
iv. Maximum power point tracking systems and
v. Hybrid system operation

1.2.1 Feasibility Study

One of the recent studies on the feasibility of a standalone solar-wind hybrid energy system for application in the region of Ethiopia shows a potential of such systems in [8]. According to the reference, the annual average irradiation in Europe is about 1000 kWh/m^2, in middle-east it's approximately around 1800 kWh/m^2. In the tropical zone the average is estimated to be around 2000 kWh/m2. Based on a variety of design parameters; such as PV size, wind turbine rotor swept area, battery capacity, PV module slope angle, and wind turbine installation height leveled cost of energy ($/kW h) ranging in between $1 and $4 have been estimated.

The installation of hybrid energy system in remote areas is one of the promising applications of renewable energy technology. Recent research and development of [9] have shown excellent potential, as a form of supplementary contribution to conventional power generation system. Combination of PV and wind in a hybrid energy system reduces the requirement of a battery bank and a diesel engine. Feasibility of hybrid PV/wind energy system strongly depends on solar radiation and wind energy potential available at the site. Optimum size of hybrid PV/wind energy system can be calculated on an hourly basis or on the basis of daily average power per month, the day of minimum PV power per month, and the day of minimum wind power per month. In the conventional approach power electronics based DC–DC converter are used for maximum energy extract from solar and wind energy sources and control the complete hybrid system. Some researchers in [9] - [10] have used different controlling technique for different combination of hybrid energy systems.

The study in [9] proposed an advanced control technique to manage the flow of energy efficiently with good power quality. The system voltage variation, the frequency, waveform and power factor at the time of grid connection, must be maintained within the limits. Hybrid energy flow can also be controlled by applying advance control techniques on power electronic converters.

Another study in [11] focuses on the application status and outlook of wind–solar hybrid energy system in China. The density of potential wind energy is more than 50 W/m^2. Wind–solar hybrid energy system is more and more considered in China as a renewable energy resource compared to conventional stand-alone wind energy system and solar

energy system. The circuit topology must be regarded to acquire the maximum power point (MPP). The conventional buck, boost and buck-boost circuit are used in the hybrid system, but the efficiency is low during the acquire MPP course. It says that some intelligent control method must be used to improve the conventional proportional-integral-derivative (PID) controller to develop an advance MPPT algorithm. The efficient MPPT algorithm must be considered to increase the output efficiency of hybrid generate system.

The study in [12] states that the climatic conditions determine the availability and magnitude of solar and wind energy at particular site. The long term performance is one of the most important design criteria for stand-alone hybrid energy systems. So, weather data containing hourly solar irradiation, wind speed and ambient temperature are required for feasibility study and design of hybrid systems.

1.2.2 Wind Energy Conversion Systems

There are significant differences between wind power and conventional power generation systems. Wind turbines employ different, often converter based generating systems. Wind is the prime mover of the wind turbines, it is not controllable and fluctuates randomly. Besides, the typical size of individual wind turbines is much smaller compared to the conventional utility generators. Due to these differences, the power generation from wind interacts differently with the network and it may have both local and system-wide impacts on the operation of the power system.

The configuration in TechnoCentre Éolien is developed with permanent magnet synchronous machine (PMSM) based wind energy conversion system and two controlled two-level voltage source converters (VSC). As described in the technical report in [13], a similar configuration is followed in this study. Typical configuration is followed where PMSM is directly coupled with a wind turbine [14]. The control access through the AC-DC-AC converters allows the electrical power to connect with the microgrid. The power converter circuits are typically made up of generator side converter, DC-link circuit and load side converter [15]. The major concern of Wind Energy Conversion System (WECS) is to control the speed of a wind turbine. A control system is required to operate the wind turbine at above rated wind speed, maintain a desired voltage level in order to control the power generation during low demand and vice versa. Speed control of wind turbine is also important to ensure the safety of the WECS, converters, transformers and loads.

Non-linear speed controller can be developed by rotor or wind speed estimation as explained in [16]. According to this study, stator flux estimation allows the system to estimate the rotor speed. A value of constant, K is chosen to achieve the best performance. The control system has been designed into two independent parts, machine side converter control and grid side converter control. Machine side converter control allows the wind turbine to operate at MPP, so that it extracts the maximum possible power generation.

Another technique to control the speed of wind turbine by pitch regulation is the use of basic PID controller [17]. To apply the PID control technique a transfer function of a

wind turbine has been derived. Non-linearities and step response of a wind turbine has been considered to derive the transfer function in order to design the PID controller for speed control.

Digital robust control technique controls the speed of a wind turbine by reducing the dynamic loads of the blades using a pitch regulation method [18]. The strategy considers the Above Rated Wind Speed (ARWS) zone. During the above rated wind speed condition, the controller regulates the pitch angle of the turbine blades thus the speed is being controlled. The controller has been designed using a discrete-time control model. This method allows the wind turbine to be operated at desired speed within the ARWS zone.

An adaptation technique can be applied to control the speed of wind turbines [19]. The adaptation strategy updates a sliding gain and a turbine torque which is unknown to the controller. A sliding mode control method has been applied by deriving a mathematical model to update the sliding gain to improve the system response. The control system tracks the speed profile to operate the wind turbine at maximum power extraction point which is also known as MPPT. Adaptive sliding mode control controls the speed of wind turbine by controlling the actual turbine torque.

1.2.3 Solar Photovoltaic Energy Conversion Systems

For the generation of electricity in remote area at reasonable price, sizing of the power supply system plays an important role. Since the scaling of input power source is easy,

solar PV systems are an excellent choice in remote areas for low and medium level power generation [10].

According to a provisional design specification of TechnoCentre Éolien, a 5kW solar PV system was proposed in [7], [13] and was integrated in hybrid energy system configuration. The given structure is this study was a standard configuration used for conventional solar PVECS. That includes a solar PV array, DC-DC buck converter, MPPT controller and loads connected through a controlled DC-AC three phase inverter. The generation side DC-DC converter is controlled with signals from maximum power point tracking (MPPT) system and the grid or load side converter is controlled with a two-level VSC.

There are two major families of PV generation system as described in [20]:

i. Grid-connected system
ii. Stand-alone system

In this research, a simulation model of stand-alone microgrid is developed based on the infrastructure in TechnoCentre Éolien. Most usual configuration of stand-alone PV system comes with an energy storage system.

The building block of PV array is solar cell, which is basically a p-n semiconductor junction that directly converts solar irradiation into DC current using the photovoltaic effect [21]. A mathematical model of solar PV cell can be obtained from the equivalent circuit. The PV module was constructed with a number of solar cells in series-parallel connection and a number of PV modules are required to make an array.

1.2.4 Maximum Power Point Tracking Algorithm

Maximum power point tracking is a technique that ensures the maximum power extraction from non-linear energy resources like solar photovoltaic, wind energy systems and tidal energies. For solar PV systems, MPPT algorithm allows the controller to follow the optimum voltage and current from a photovoltaic module. Most widely used MPPT algorithms are:

a. Constant voltage method
b. Perturb & Observe (P&O) method
c. Incremental conductance method

a. Constant Voltage Method

Although this method is very simple, it is always difficult to select the optimal value of constant *K*, that reduces the efficiency of power generation [22]. The basis of the constant voltage algorithm is an observation from current-voltage (I-V) characteristic curve, the ratio of the PV array's maximum power voltage, V_{MPP} to its open-circuit voltage, V_{OC} that is approximately constant [23]. In other words: $(V_{MPP} / V_{OC}) \approx K < 1$. The MPPT calculates the correct operating point using this relationship between V_{MPP} & V_{OC} and adjusts the array voltage until it reaches the MPP with a pre-set value of *K*. The operation is repeated periodically to track the MPP position.

b. Perturb & Observe (P&O) Method

This method is also known as Hill Climbing (HC) method [22]. Its working principle is making a small active voltage perturbation in a certain working voltage of photovoltaic

cells and observing the change direction of output power. Disturbance observation has been widely used in photovoltaic maximum power point tracking because of its simple control structure. However, due to its fixed step, the oscillation phenomenon occurs near the maximum power point, which reduces the efficiency of power generation.

In the P&O algorithm, the operating voltage of the PV array is perturbed by a small increment, and the resulting power change (ΔP) is measured [23]. If ΔP is positive, then the perturbation of the operating voltage moved the PV array's operating point closer to the MPP. The advantage of this method is its simplicity and that is easy to implement. The P&O method has a limitation to track the MPP when the sunlight decreases, because the power-voltage (P-V) characteristic curve flattens out. Another fundamental drawback of P&O method is that it cannot determine when it has actually reached the MPP.

c. Incremental Conductance Method

This method estimates the relation between the operating point voltage, U and the maximum power point voltage, U_{max} [24]. The method of increasing conductivity follows three conditions: $U < U_{max}$, $U > U_{max}$ *and* $U = U_{max}$. To realize the position of maximum power point a reference voltage U_{ref} is applied. For a light intensity and outside temperature variation, the incremental conductance method could control the output voltage to track the maximum power point voltage smoothly and could also reduce oscillation phenomena near the maximum power point. However, this control algorithm is very complex, and the setting of adjusting voltage ΔU influences the maximum power point tracking accuracy greatly.

In another study a terminal sliding mode control (TSMC) algorithm has been applied to achieve the MPP under the changing atmosphere [25]. Here, a module current (i_{pv}) and a voltage (V_{pv}) are measured from PV array and sent to the MPP searching algorithm that generates the reference maximum power voltage, V_{pvd}. Then, the reference voltage, V_{pvd}, is given to the MPV-based TSMC algorithm for the maximum power tracking. To achieve the maximum power tracking, the terminal sliding mode controller is proposed to let PV voltage V_{pv} track the reference MPV V_{pvd}.

The incremental conductance algorithm starts with measuring the present values of PV module voltage, V, and current, I [22]. Then, it calculates the incremental changes in current (dI) and voltage (dV) using the present values of current and voltage respectively. The incremental conductance algorithm is derived by differentiating the PV array power with respect to voltage and setting the result equal to zero. A primary advantage of the incremental conductance over the perturb-and-observe algorithm is that the incremental conductance can actually calculate the direction in which to perturb the array's operating point to reach the MPP [23]. It can determine when it has actually reached the MPP. Thus, under rapidly changing conditions, it should not track in the wrong direction, as P&O can, and it should not oscillate about the MPP once it reaches it. Based on the above literature review on MPPT algorithms for solar PV systems, a comparative analysis between the methods is summarized below.

Table 1 Comparison between the types of MPPT algorithms

	Constant Voltage (CV)	***Perturb & Observe (P&O)***	***Incremental Conductance***
Method	Open Circuit Voltage	Hill Climbing	Hill Climbing
Response Time	Fast	Faster	Slow
Efficiency (approx.)	73-85%	81.5-85%	88-89.9%
Accuracy	Low	High	Higher

According to the analysis, the incremental conductance method shows higher accuracy and promising efficiency, though the response time is slower compared to other methods. So far the incremental conductance method is the preferable one for the MPPT algorithm of PVECS.

1.2.5 Hybrid Operation

A Hybrid Solar-Wind System Optimization Sizing (HSWOS) model was developed to optimize the capacity sizes of different components of solar-wind hybrid energy system in [26]. It employs a battery bank to store the power generated. Mathematical modeling of a solar photovoltaic module, wind turbine and storage bank was discussed to simulate the behavior of the solar-wind hybrid energy system. The economic model based on the Levelized Cost of Energy (LCE) model has been proposed to understand the cost

effectiveness of the system. An optimum combination of a hybrid solar wind energy system must satisfy both the reliable and economical requirements.

In hybrid operation of solar-wind system, wind energy is often given priority since the availability of wind is greater. A basic power management is proposed in [27] where wind is given priority over solar PV. Solar PV system can be operated in the daytime when it is possible to operate the wind turbines both during day and night time [28]. A strong strategic control algorithm can not only ensure the full use of solar-wind energy resources, but also stabilizes the output current of the system and reduces the volatility and impact on energy storage [29].

Jian et al. [30] suggests that wind-solar hybrid system can be classified into three systems based on the bus bar forms, including pure AC bus bar, pure DC bus bar and hybrid AC-DC bus bar system. To simplify the system according to the infrastructure available in TechnoCentre Éolien, a pure AC bus bar system is developed in this work.

1.3 Objectives, Scopes and Contributions

The main objectives of the thesis concentrate on developing following:

1) A simulation model for solar photovoltaic energy conversion system (PVECS), wind energy conversion system (WECS), diesel generation system and apply maximum power point tracking algorithm to extract maximum power.
2) A simulation model for stand-alone solar-wind-diesel hybrid energy system (SWDHES).
3) Control systems to improve the power quality of the generated power from hybrid operation.
4) A power management system to share the power generated by the hybrid system, to increase the system reliability and reduce the use of diesel. Voltage and frequency regulation systems are developed and implemented into the simulations model.

Thesis contribution: A part of the research infrastructure at TechnoCentre Éolien focuses on the integration of a solar PV with a wind energy conversion system and developing of a control strategy for the power system feeding a microgrid. A power management strategy is required to operate such hybrid system. This research is conducted based on the infrastructure developed in Gaspé, so TechnoCentre Éolien may apply the algorithm for the hybrid operation. The main contribution of this research is presented in chapter 2, 3 and 4.

1.4 Organization of the Dissertation

Chapter 2 focuses on the development of solar photovoltaic energy conversion system (PVECS) that includes a background on the fundamentals of PVECS, modeling solar cell, module and PV array. It introduces the major components of PVECS, control schemes and the configuration developed in this work.

Chapter 3 describes the principle of wind energy conversion system (WECS) that includes brief introduction to the major components of WECS, modeling wind turbine and the energy conversion system. It describes control schemes for wind turbine and the electrical configuration developed based on practical setup. It covers general background on diesel generators and methodology applied to develop the system.

In **chapter 4** a power management strategy is developed for the hybrid operation of stand-alone solar-wind-diesel energy conversion system. The integration of energy storage is also introduced in this chapter. It also provides the result obtained from simulation study.

Chapter 5 concludes the contribution of this work and provides an overview on the development of stand-alone hybrid energy systems.

Chapter 2

2 Solar Photovoltaic Energy Conversion System

2.1 Introduction

The concept of using renewable energy sources emerged from the need to search for alternate green sources of energy. In order to diminish the greenhouse effect and to slow the depletion of fossil fuel, the solar energy has been utilized [31]. Photovoltaic power systems are becoming increasingly important in modern electrical grids.

This chapter presents a mathematical model of solar PV cell that is based on the equivalent circuit [32], [33]. The model was applied to in simulation in order to generate the behaviour of a 250W PV module. The results are compared to the original characteristic curves from the datasheet of the CS6P-250M module [34]. This model can generate the I-V and P-V characteristics of the PV cell and module. It is developed to study the effects of different parameters on the output of PV module. The model uses the Matlab®/Simulink® interface to simulate and to obtain the simulation results. It can also be applied for further simulation based research and analysis on PVECS.

2.2 Background

In recent years, PV power systems have drawn significant research attention in modeling and simulation studies for both stand-alone and grid-tied systems [35]. Simulation based

implementation is being widely popular in research, especially for large scale analysis. The PV module is the basic building block in the PV systems. The conventional technique to model the solar cell is to establish the mathematical expressions based on the equivalent circuits of the cell [36]. A solar cell consists of layers of semiconductor materials that exploit the photoelectric effect to convert photon energy of the sun radiation into electricity. In terms of power electronics, a solar cell can be considered as a current source with non-linear characteristics [37].

The study [37] includes the performance analysis of a 250W PV module and its behavior on different air temperature conditions, irradiance levels. It also focuses on the effects of varying shunt and series resistances. The model has been developed considering possible environmental effects on solar PV generation. The data from the characteristics curves obtained in this study is compared to the curves provided by the CS6P-250M PV module datasheet. Therefore, it is possible to simulate the behavior of any large scale PV array or solar PVECS using the model developed in this research.

2.3 Photovoltaic Cell

2.3.1 Modeling PV Cell

The equivalent circuit of a solar photovoltaic (PV) cell is given below. It includes a current source *(I_{PH})*, a diode *(D)*, a shunt resistance *(R_{SH})* and a series resistance *(R_S)* [38], [39].

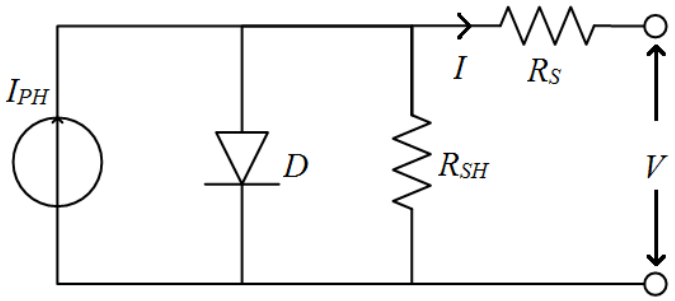

Figure 2 Equivalent circuit of a solar photovoltaic cell

An equation of current to the load can be obtained from the equivalent circuit in fig. 2. The load current equation is given below [22], [32], [40]:

$$I = I_{PH} - I_S \left[exp \frac{q(V+IR_S)}{NKT} - 1 \right] - \frac{(V+IR_S)}{R_{SH}} \quad (1)$$

Where, I is the load current, I_{PH} is the photocurrent, I_S is the diode saturation current, q is the electron charge, V is the terminal voltage of the cell, N is the diode ideality factor, K is the Boltzmann constant, T is the cell temperature, R_S and R_{SH} is the series and shunt resistance respectively. The behavior of a solar photovoltaic (PV) cell is completely dependent on these parameters.

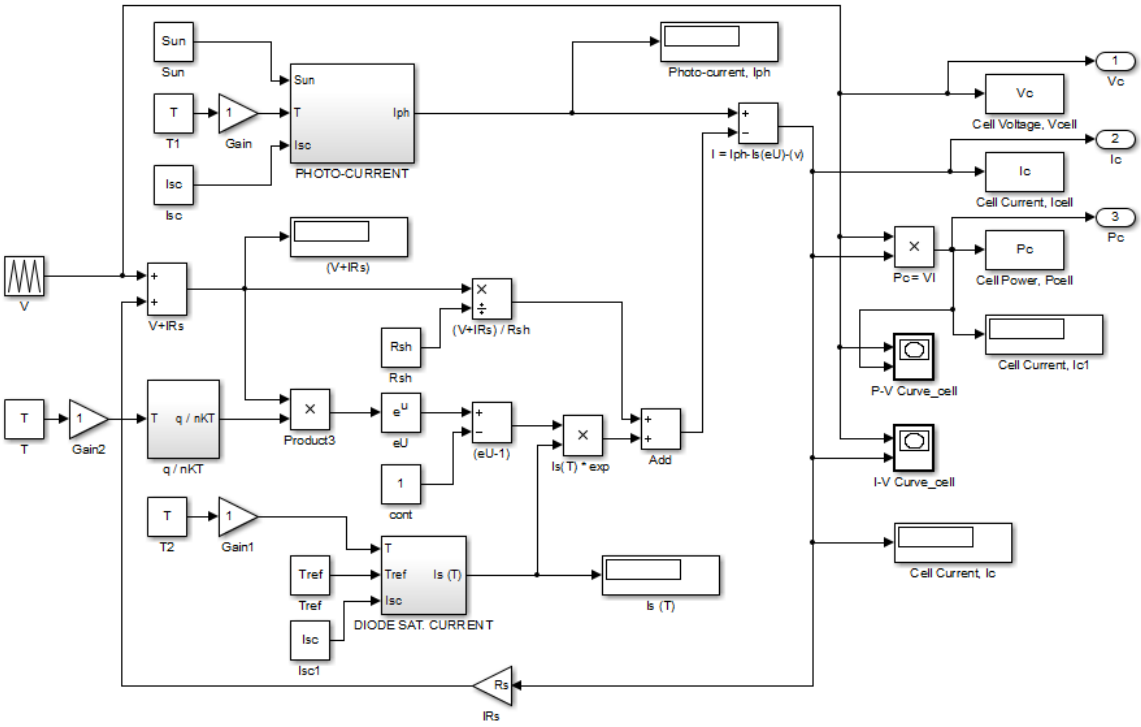

Figure 3 Simulation model subsystem of solar PV cell

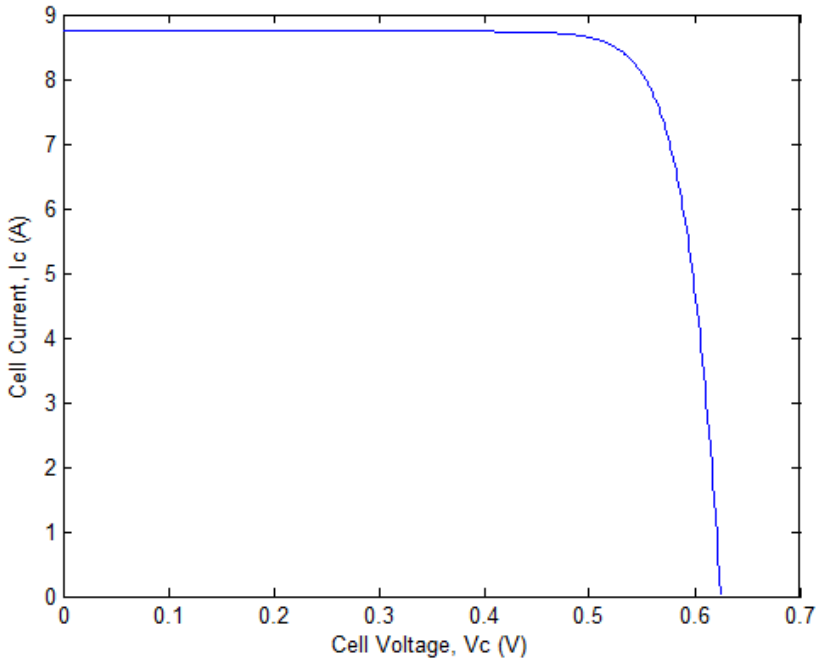

Figure 4 Current vs voltage (I-V) curve of simulated PV cell

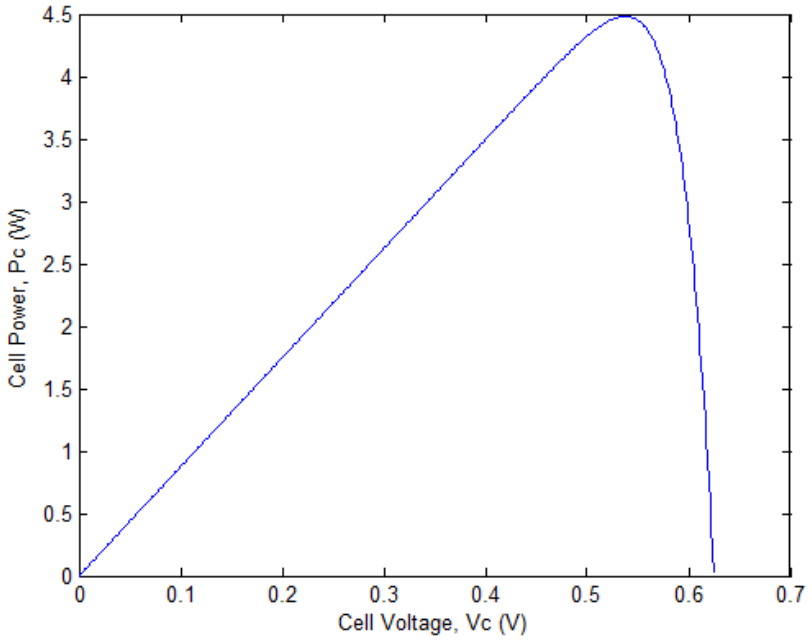

Figure 5 Power vs voltage (P-V) curve of simulated PV cell

Fig. 3 shows the Simulink® subsystem for solar PV cell. The I-V characteristics (current vs voltage) curve generated from the simulation model of a solar PV cell is shown in fig. 4. The current remains steady until the cell voltage reaches at 0.5 V and drops when the voltage reaches its saturation point at 0.62 V. Fig. 5 shows the P-V characteristics (power vs voltage) curve where the cell power develops with the increase in voltage until the voltage reaches at maximum power point when the cell voltage is 0.55 V approximately. The power starts to drops when the voltage is above MPP.

2.4 Photovoltaic Module

2.4.1 Modeling PV Module

In order to develop the model of a 250 W solar photovoltaic module a real PV module CS6P-250M manufactured by *Canadian Solar* has been considered as a standard module.

The model was developed based on the available information from the datasheet. Following table shows the key specification of the PV module under Standard Test Conditions (STC) [34].

Table 2 Key specification of CS6P-250M PV module under STC

Electrical Characteristics	**CS6P-250M**
Nominal Maximum Power	250 W
Optimum Operating Voltage	30.4 V
Optimum Operating Current	8.22 A
Open Circuit Voltage, V_{OC}	37.5 V
Short Circuit Current, I_{SC}	8.74 A
Temperature Coefficient of I_{SC}, K_i	0.005 $A/^0C$

The original PV module contains total 60 cells. In order to generate the specified voltage from the simulated model, total 60 cells are required to be connected in series. In this system, desired voltage level is achieved by applying a gain on the cell voltage, equals to the number of total cells, to develop the model of a 250 W PV module.

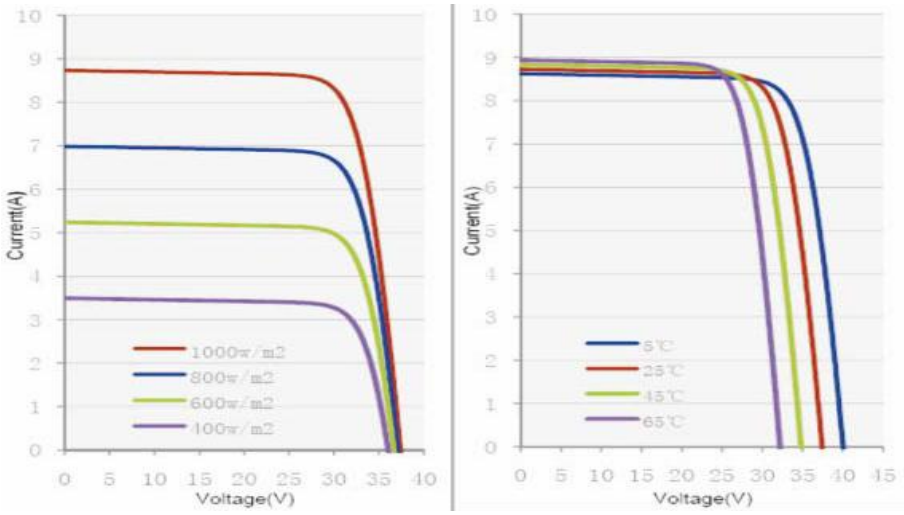

Figure 6 I-V characteristics of module for different irradiation and temperature

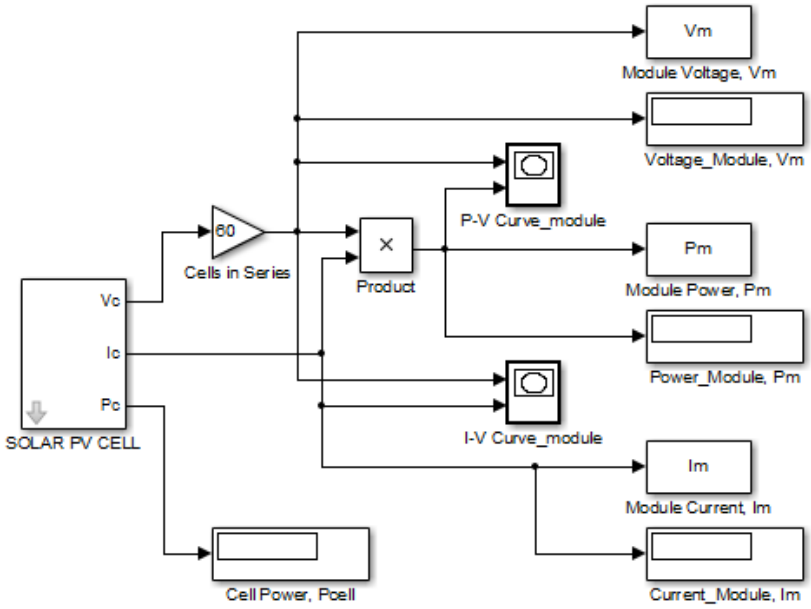

Figure 7 Simulation model of solar PV module

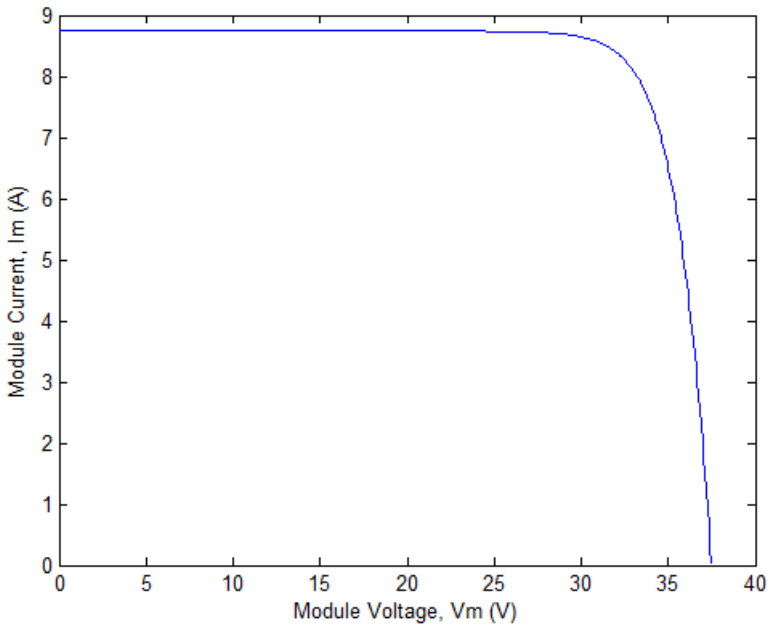

Figure 8 I-V curve of simulated PV module

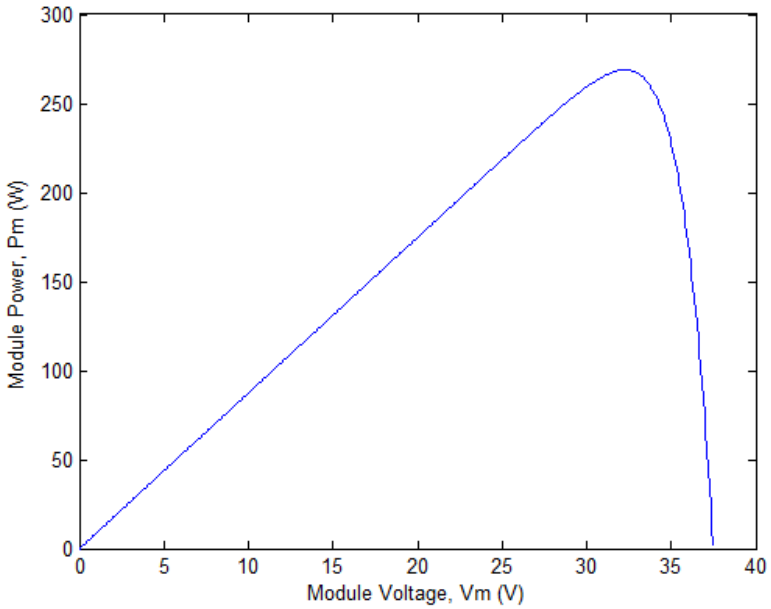

Figure 9 P-V curve of simulated PV module

Fig. 6 shows the I-V curve of the CS6P-250M module for different irradiation and temperature [34]. The Simulink® model of the PV module, I-V and P-V characteristics curves from the simulation are given in fig. 7, 8 and 9 respectively. The results in fig. 8 and 9 are obtained under STC. The characteristic from the CS6P-250M as shown in fig. 6 is compared with the results obtained from the simulation and presented in fig. 11 and 12.

2.4.2 Effect of Solar Irradiance Variation

The model of PV cell in fig. 3 includes two major subsystems that play a great effect on the behavior of PV module. One of them calculates the photocurrent, I_{PH}. The photocurrent, I_{PH} depends on the solar irradiance and cell temperature. The output of the PV module varies as a function of solar irradiance level which can be obtained from the following equation [22], [32], [40]:

$$I_{PH} = [I_{SC} + K_i(T - T_{ref})]\frac{B}{1000} \quad (2)$$

Here, I_{SC} is the short circuit current, K_i is the temperature coefficient of short circuit current, T is the cell temperature, T_{ref} is the reference temperature and B is the solar irradiation.

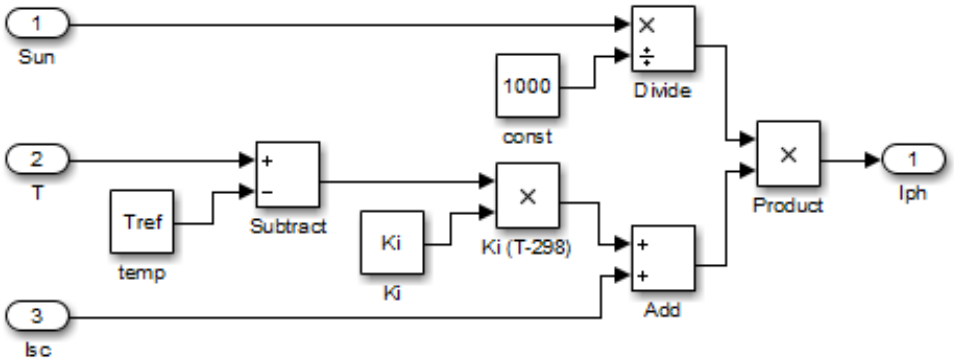

Figure 10 Subsystem of simulation model for photocurrent

Fig. 10 shows the subsystem that calculates the photocurrent. The simulation was performed for 1000, 800, 600 and 400 W/m^2 irradiation levels under the STC. Cell temperature, *T* was kept constant at 25^o C (298 K).

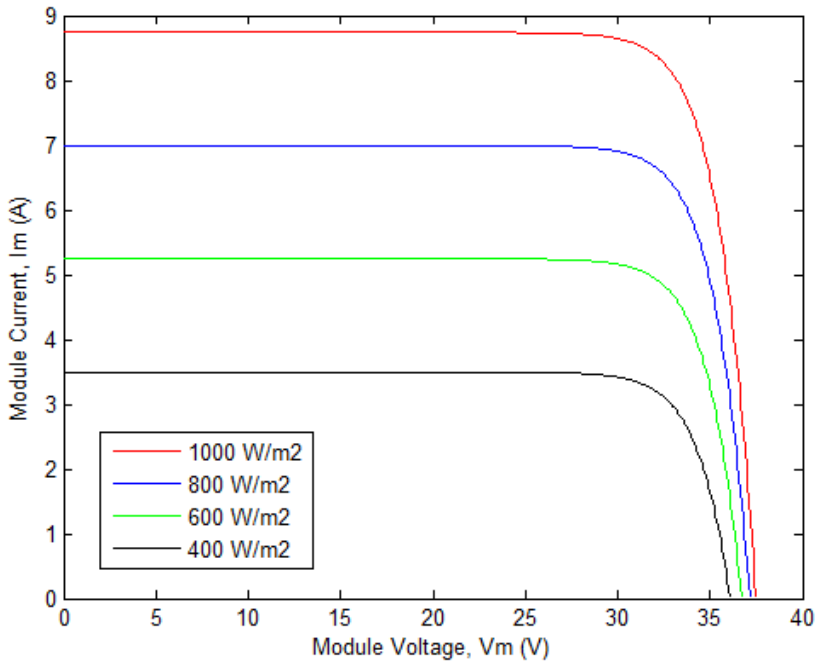

Figure 11 I-V curve of the PV module for different irradiance level

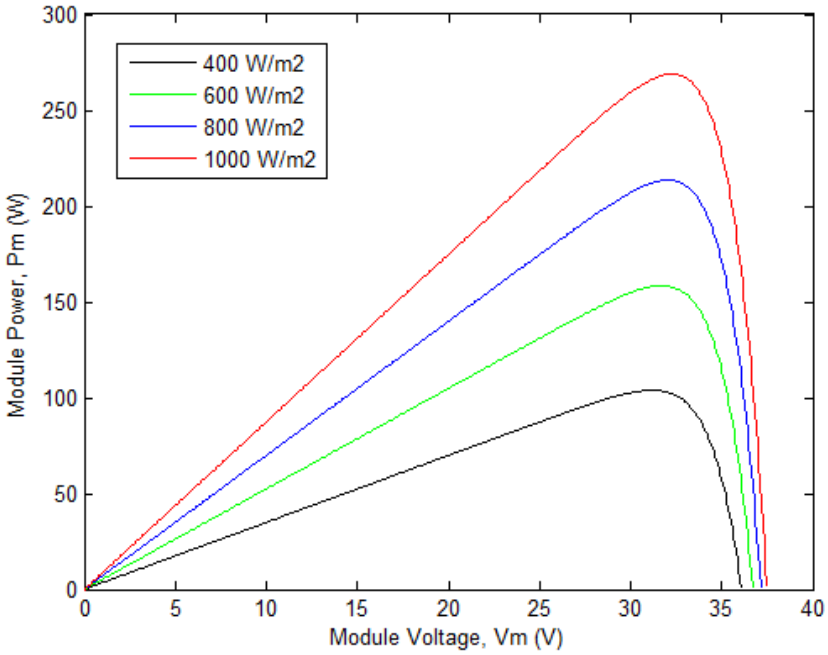

Figure 12 P-V curve of the PV module for different irradiance level

The effects of different irradiation level on I-V and P-V characteristics are presented in fig. 11 and 12 respectively. As seen in fig. 11 and 12, the variation of irradiation level affects widely on the current and voltage generated in PV module. According to the results; open circuit voltage, V_{OC} drops slightly and short circuit current, I_{SC} decreases widely with the decrement of solar irradiation, *B*. This behavior for different solar irradiation has been validated from the datasheet of the CS6P-250M PV module and fig. 6 [34].

2.4.3 Effect of Temperature Variation

The other subsystem of PV cell model calculates the diode saturation current, I_S. The diode saturation current varies as a cubic function of the temperature and it can be expressed as the following equation [32], [41], [42]:

$$I_S(T) = I_{RS}\left(\frac{T}{T_{ref}}\right)^{\frac{3}{N}} e^{-\frac{qV_t}{NK\left(\frac{1}{T}-\frac{1}{T_{ref}}\right)}} \tag{3}$$

In this equation, I_{RS} is the diode reverse saturation current and V_t is the thermal voltage. The cell reverse saturation current can be obtained from the equation given below [41]:

$$I_{RS} = \frac{I_{SC}}{[e^{qV_{OC}/NKT}]} \tag{4}$$

Thermal voltage, V_t can be obtained from the following equation:

$$V_t = \frac{KT}{q} \tag{5}$$

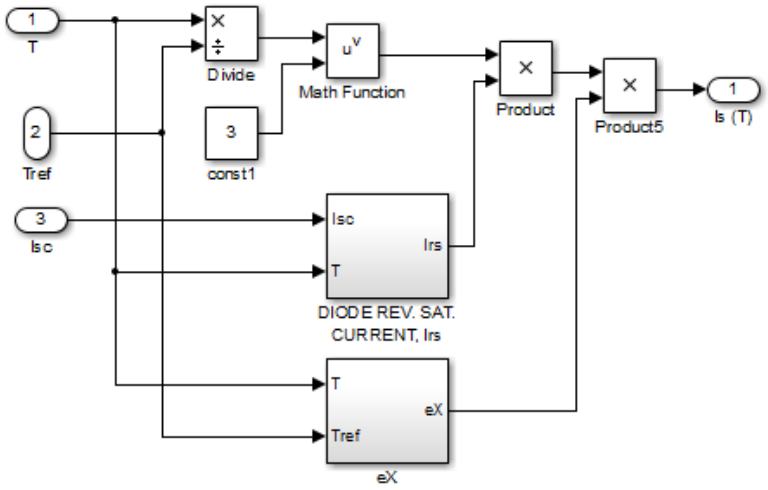

Figure 13 Subsystem of simulation model for diode saturation current

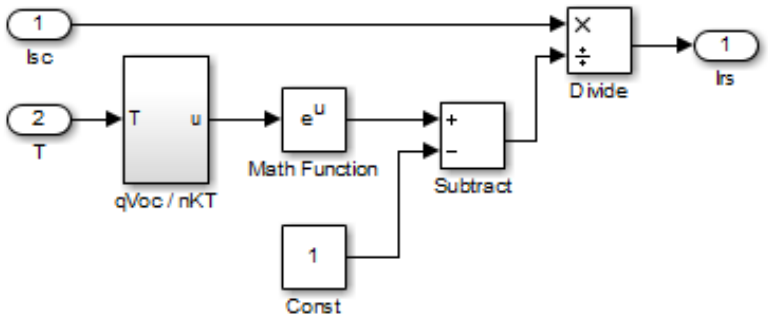

Figure 14 Subsystem of simulation model for reverse saturation current

The subsystems showed on fig. 13 and 14 are constructed to generate the saturation current, I_S and reverse saturation current, I_{RS} based on (3) and (4) respectively. The simulation was performed for 5° C (278 K), 25° C (298 K), 45° C (318 K) and 65° C (338 K) under the Standard Test Conditions (STC). During this test solar irradiance, *B* was kept constant at 1000 W/m^2.

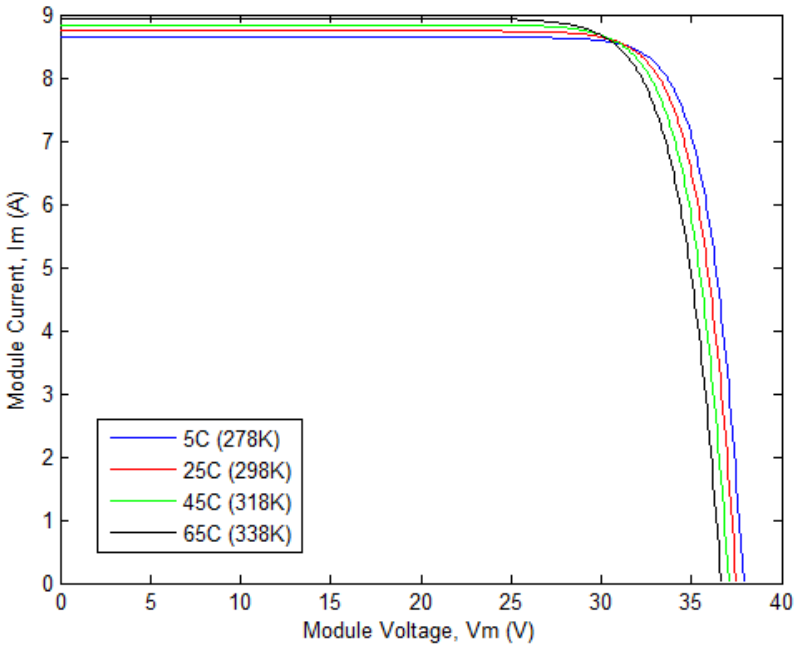

Figure 15 I-V curve of the PV module for different temperature level

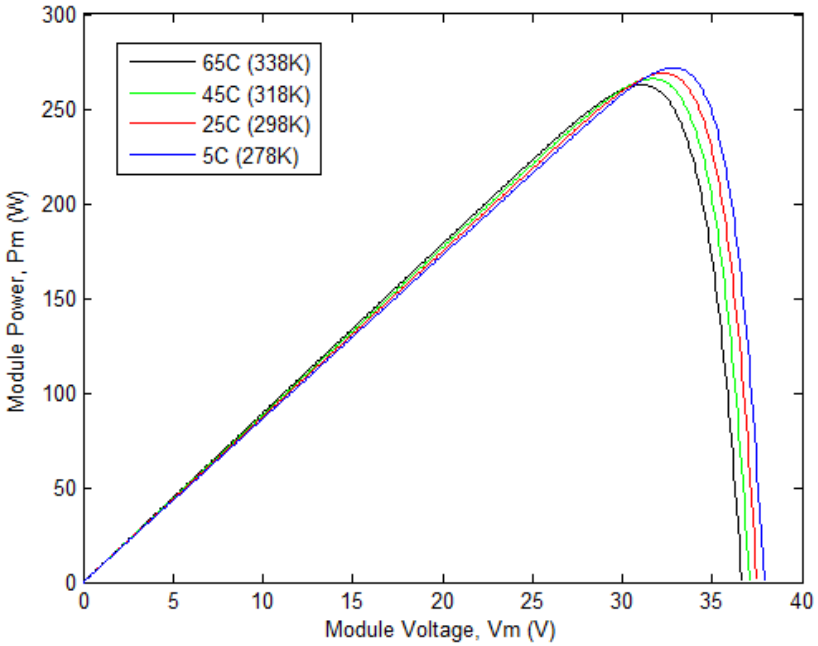

Figure 16 I-V curve of the PV module for different temperature level

The effects of different temperature on I-V and P-V characteristics are presented on fig. 15 and 16 respectively. According to the I-V and P-V characteristics in Fig. 15 and 16; open circuit voltage, V_{OC} drops and short circuit current, I_{SC} rises slightly when the temperature increases. This behavior for varying temperature has been validated from the datasheet of the CS6P-250M PV module and fig. 6 [34].

2.4.4 Effect of Varying Series Resistance

Generally, the typical value of series resistance, R_S of the PV cell is very low. This model was developed to render the suitable model for any given PV cell so that it is possible to vary R_S and observe its effects on the behavior of the PV module. This simulation was performed for three different values of R_S, respectively 1 mΩ, 5 mΩ and 10 mΩ. The

simulation was performed under STC, where temperature, T was kept constant at 25^{o} C (298 K) and solar irradiation level, B was kept constant at 1000 W/m^{2}.

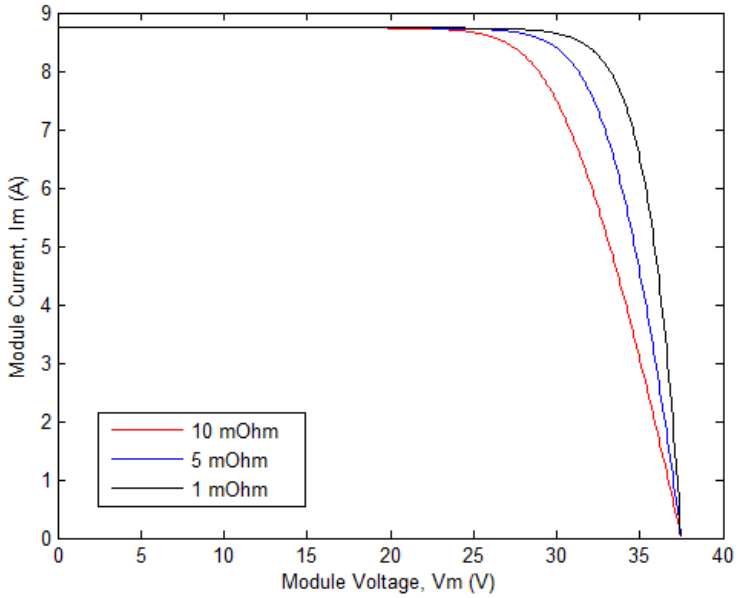

Figure 17 I-V characteristics of PV module for different values of series resistance R_S

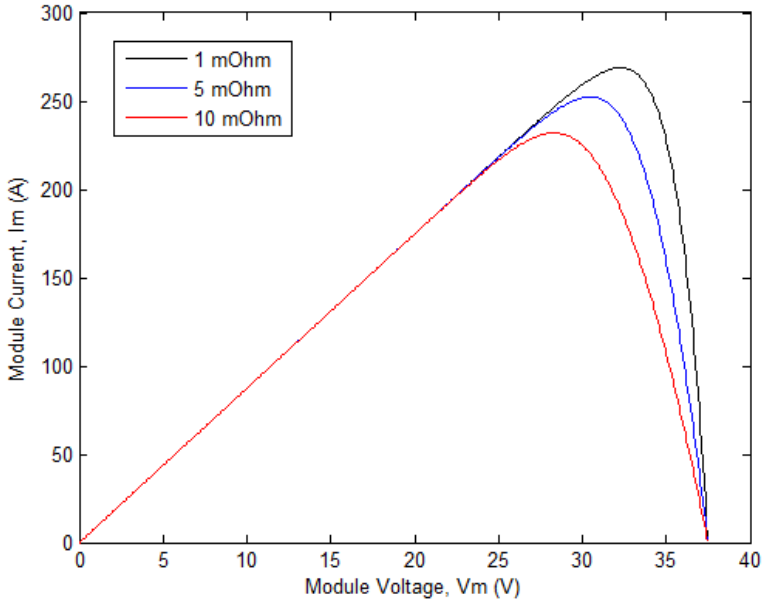

Figure 18 P-V characteristics of PV module for different values of series resistance R_S

As seen in fig. 17 and 18, the variation of R_S affects the deviation of maximum power point of the PV cell and the module as well. However, the open circuit voltage, V_{OC} and short circuit current, I_{SC} remains same.

2.4.5 Effect of Varying Shunt Resistance

In general, the value of the shunt resistance, R_{SH} of the PV cell should be large enough to achieve the maximum output from the PV module.

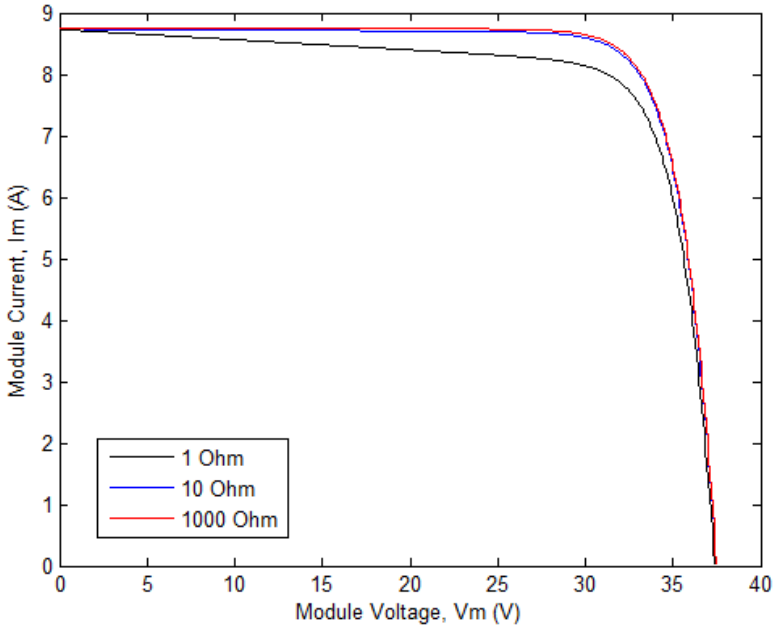

Figure 19 I-V characteristics of PV module for different values of shunt resistance R_{SH}

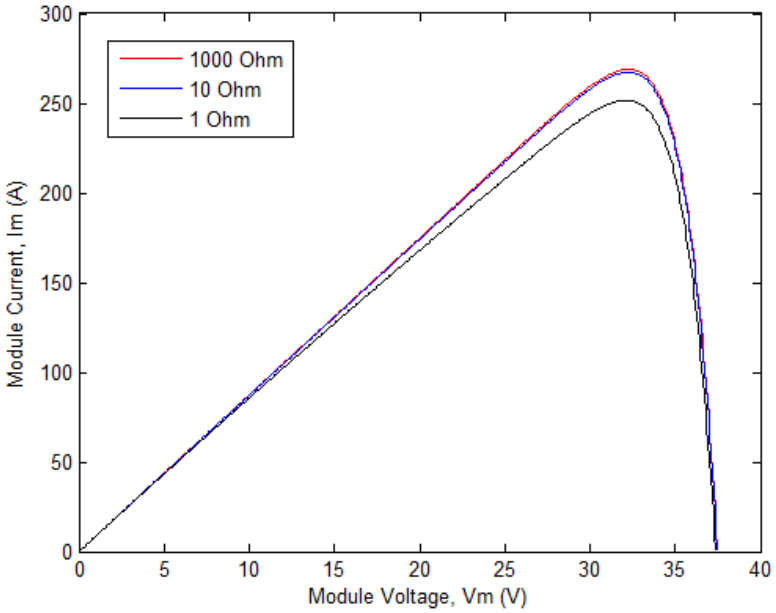

Figure 20 P-V characteristics of PV module for different values of shunt resistance R_{SH}

The effects of varying R_{SH} on module's I-V and P-V characteristics are shown in fig. 19 and 20 respectively. For low value of R_{SH}, the output current of the PV cell drops so fast and it causes a high power loss. The simulation is performed for three different values of R_{SH}, respectively 1 Ω, 10 Ω and 1000 Ω. The effects of different R_{SH} can be seen in the I-V and P-V characteristics curve of the PV module shown in fig. 19 and 20. Variation of R_{SH} also affects the deviation of maximum power point of the PV cell and module as well.

2.5 Major Components of Photovoltaic Energy Conversion System

2.5.1 Photovoltaic Array

A series parallel combination of PV module is developed to construct the model of photovoltaic array in simulation. In order to create a 6kW PV array, the CS6P-250M PV

module is applied where the nominal voltage and current generated by each module is 30.4 V and 8.22 A respectively. A bank of four modules in series generates a voltage of 121.6 V and a bank of six modules in series generates a total current of 49.32 A. The schematic diagram of series-parallel connections of PV module is shown in the fig. 21.

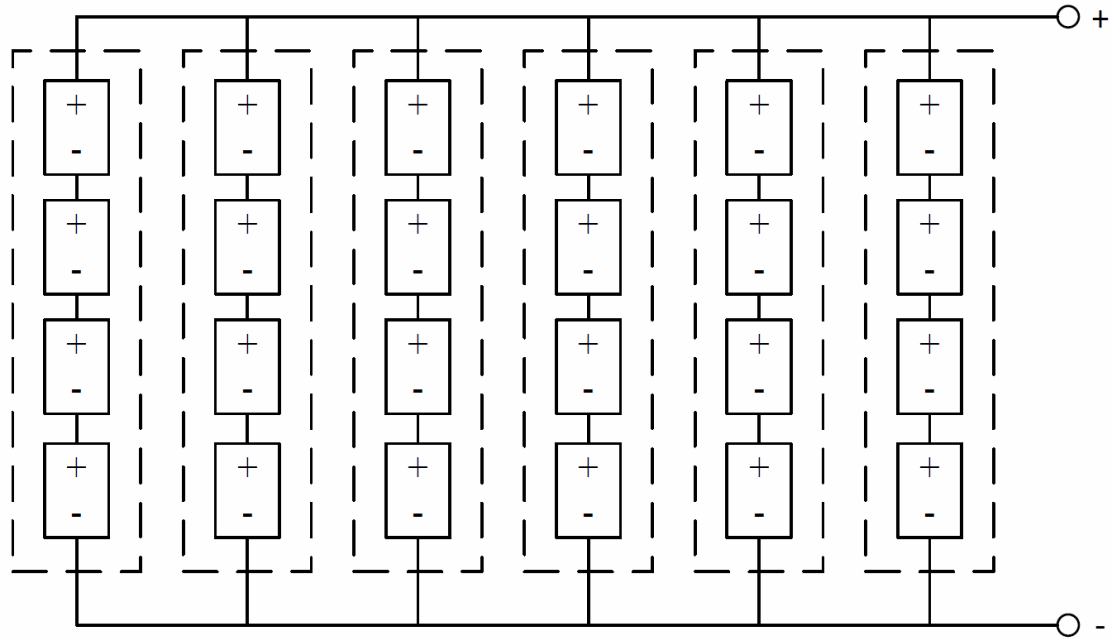

Figure 21 The schematic diagram of module connections in PV array

Total 24 PV modules are connected in a way, so that the array generates 6kW electrical power at optimal condition. Based on equation (1) to (5), a simulation model of 6kW solar PV array is constructed in Matlab®/Simulink® [43]. Fig. 22 shows the subsystem of simulation model for PV array:

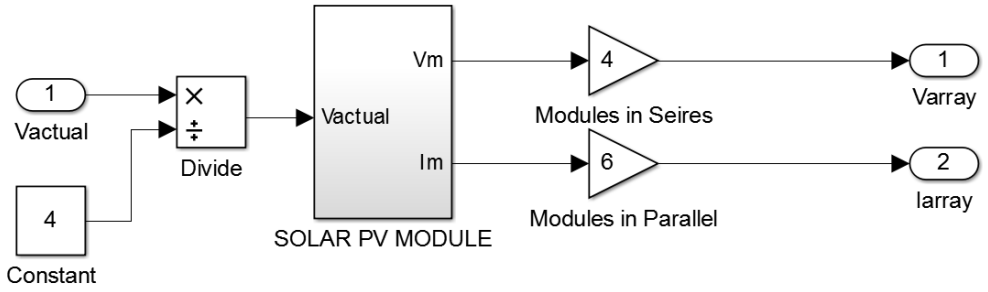

Figure 22 Subsystem of simulation model for PV array

The conventional configuration is followed to develop a stand-alone PVECS. The simulation model is developed for the case of stand-alone solar photovoltaic system. The PVECS configuration is developed with a PV array, a MPPT controlled DC/DC boost converter, a three-phase two-level VSC controlled by load voltage regulator, dump load based frequency regulator and main load. A brief discussion on dump load based frequency regulation and load voltage regulator is provided in chapter 4. The schematic and subsystem of the model is shown in fig. 23 and 24 respectively.

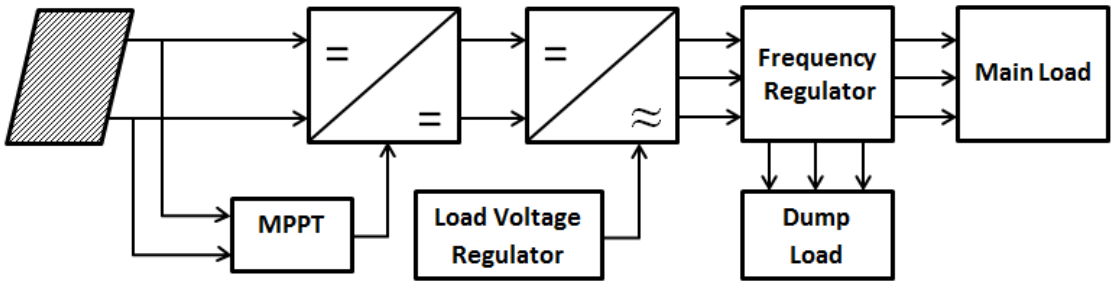

Figure 23 Schematic diagram of a stand-alone PVECS

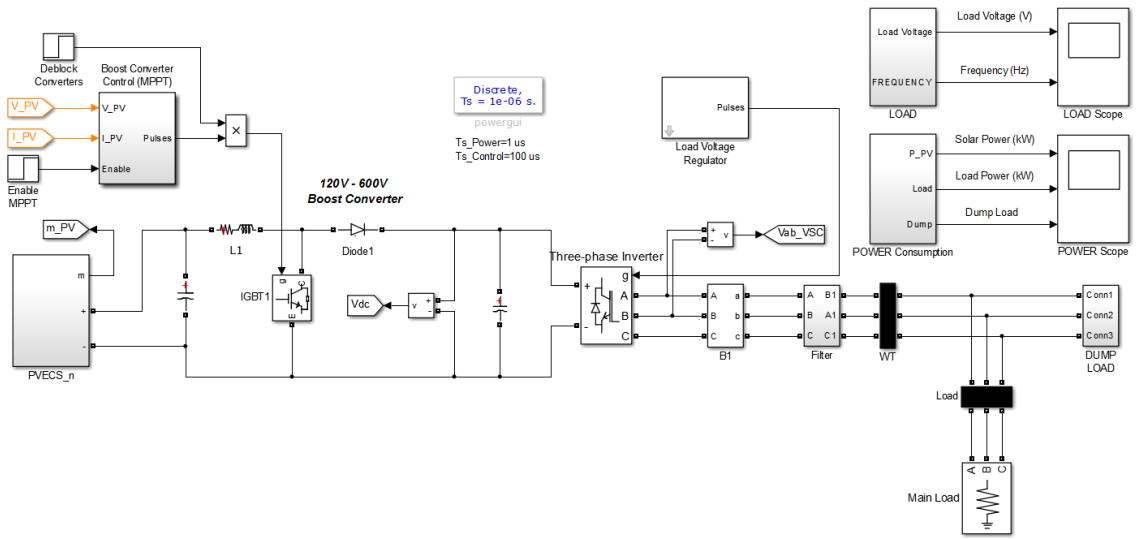

Figure 24 Simulation model of stand-alone PVECS in Simulink®/SimPower® interface

This simulation is executed for 10 seconds with variable solar irradiance and under STC where cell temperature is 25^{o} C. Results obtained from the simulation are presented below:

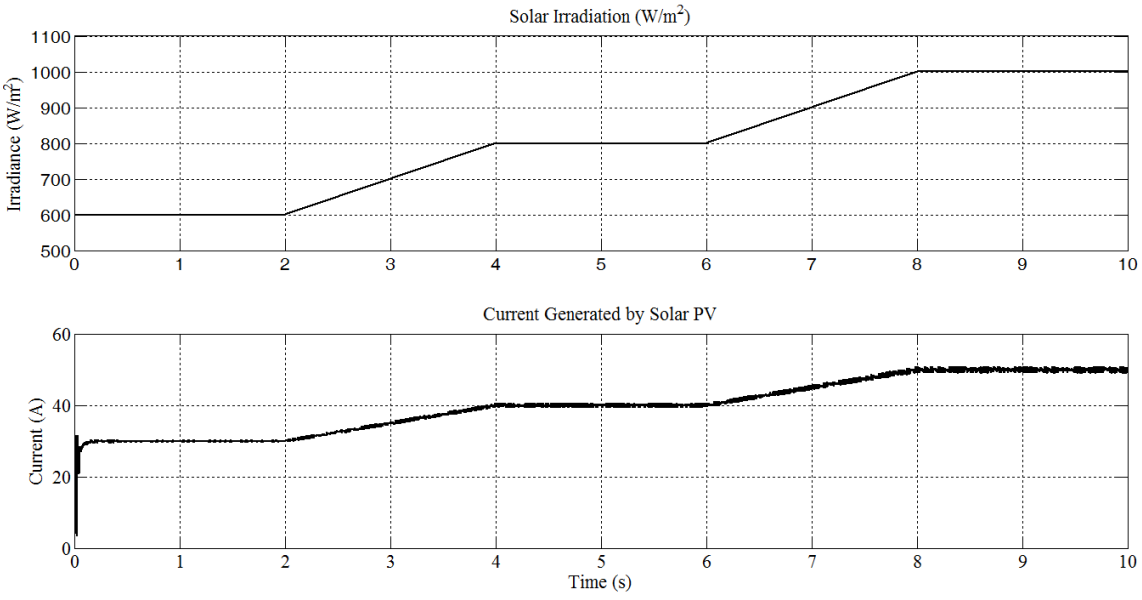

Figure 25 Variable solar irradiation (W/m^2) and current generated by solar PV

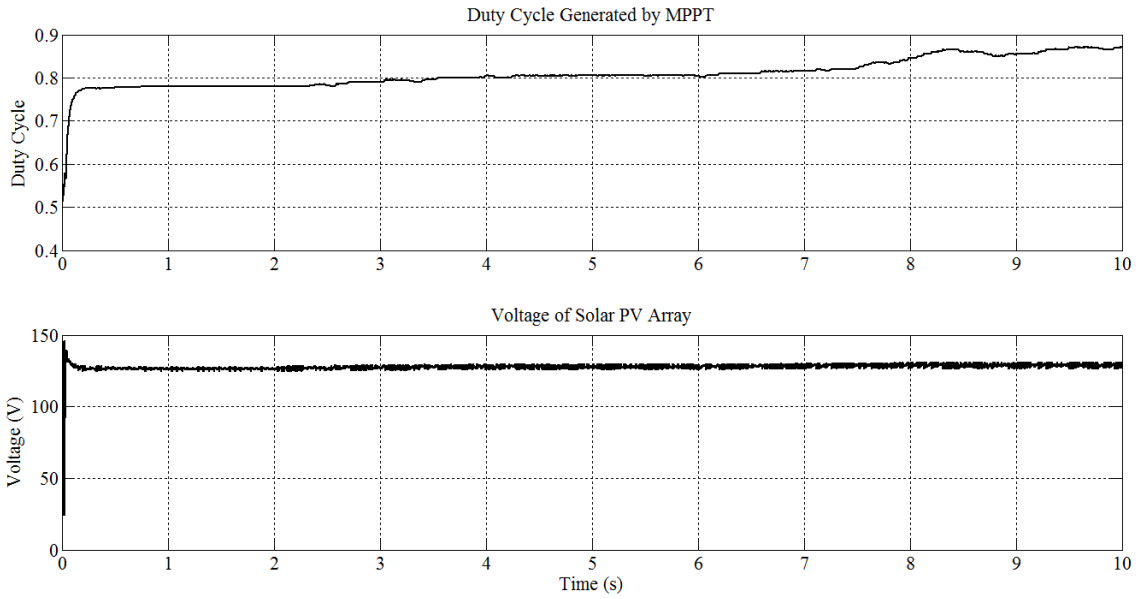

Figure 26 Duty cycle generated by MPPT and voltage induced by solar PV array

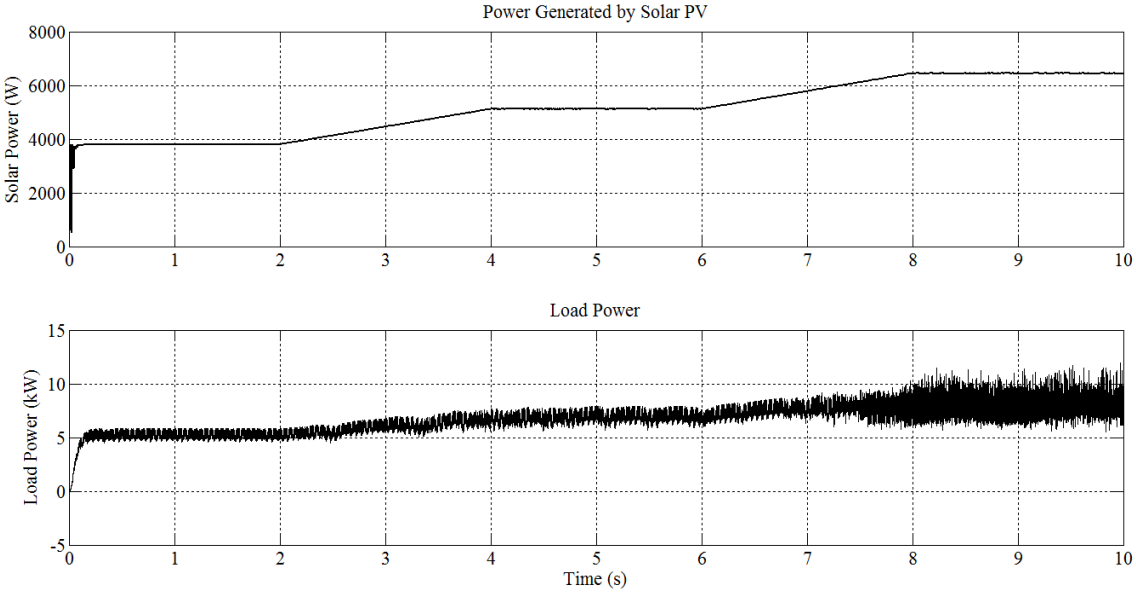

Figure 27 Power Generated by solar PV (W) and load power (kW)

Fig. 25 shows the variable solar irradiance applied to the system and generated current following the variation of irradiation. In this simulation, solar irradiation varies from 600

to 1000 W/m^2 and the generated current varies in a limit from 30 A to 50 A approximately depending on the solar irradiation. A MPPT controller, based on incremental conductance method, calculates the proper duty cycle to generate switching pulse signals for the DC/DC boost converter. Fig. 26 states the duty cycle and voltage induced at solar PV array. Total power generated by solar PV and the power consumed by resistive load is presented in fig. 27.

2.5.2 Power Electronic Converter Interface

Power electronic converters are widely used in renewable energy applications, especially for solar and wind energy systems [44]. Furthermore, power electronic converter allows accessing and controlling the torque, speed for wind turbine and voltage of solar PV in order to regulate the generated power.

Since the power generated by solar PV is DC, a classic DC/DC boost converter is applied to regulate the DC link voltage. MPPT controller generates duty cycle in order to create pulse width modulation (PWM) switching signals for the converter. The switching signal allows the boost converter to operate the solar PV system at optimum voltage and current so that the maximum power extraction is possible. The voltage induced in this PV generation end is 121.6 V, so a boost converter is required to synchronize with the micro-grid where the bus voltage is 600 V. A DC/AC three phase inverter is applied to connect the system with AC loads.

2.5.2.1 Three-phase, Two-Level Voltage Source Converter

This type of converter has been widely used in industry form different applications including solar and wind energy systems. Depending on the voltage of the device and required supply voltage the two-level voltage source converter (VSC) allows the switches to be connected in series [45]. The converter is composed of six switches, S1 to S6, with an antiparallel free-wheeling diode for each switch as shown in fig. 28 [44]. Depending on operation type and power range these switches can be IGBT, MOSFET or IGCT devices. If the primary end of the converter takes input as DC then the secondary end produces three-phase variable voltage with variable frequency on AC side. Whether this type of configuration is often referred as inverter and connects the system to AC loads, VSC circuit allows bidirectional flow of power.

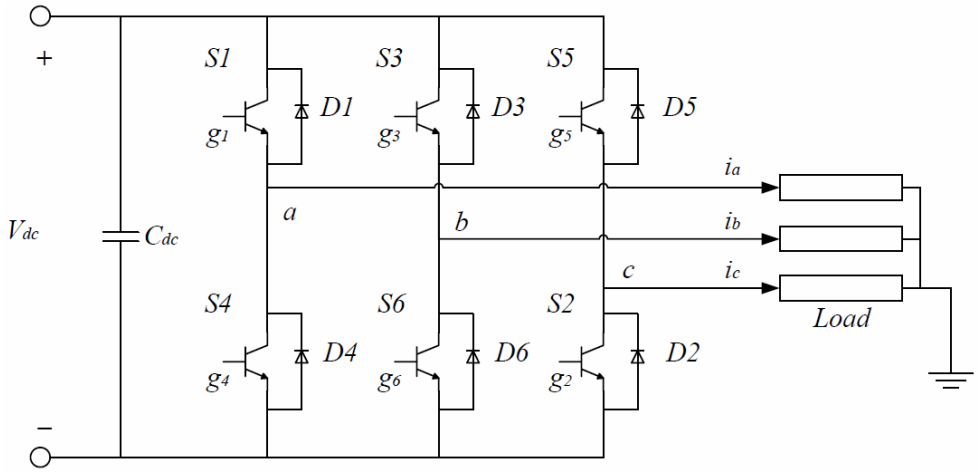

Figure 28 Circuit diagram of a three-phase, two-level voltage source converter

2.6 Development of Control Systems for PVECS

2.6.1 Maximum Power Point Tracking Control

Maximum power point tracking (MPPT) is a technique that ensures the maximum power extraction from non-linear energy sources like solar PV systems. The algorithm allows the controller to operate PV module at optimum voltage and current so the extraction of maximum power is ensured. There are many methods for maximum power point tracking. Most common methods for solar PV systems are [22], [23], [25]:

1. Constant voltage method
2. Perturb and Observe (P&O) method and
3. Incremental conductance method

Among several MPPT algorithms incremental conductance method is recommended due to higher accuracy and reliability [22], [23], [25]. This method estimates the relation between the operating voltage U and maximum voltage U_{max} [24]. Method of increasing conductivity follows three conditions: $U < U_{max}$, $U > U_{max}$ and $U = U_{max}$. To realize the maximum power point (MPP) a reference voltage, U_{ref} is applied. When the solar irradiance and outside temperature changes, the incremental conductance method controls the output voltage to track the maximum power point voltage smoothly and also reduces the oscillation phenomenon near the MPP. The flowchart of the algorithm is shown in fig. 29. The method can be expressed like following;

$$\frac{dI}{dU} = -\frac{I}{U};\ \left(\frac{dP}{dU} = 0\right) \text{ at MPP thus } U = U_{max} \tag{6}$$

$$\frac{dI}{dU} > -\frac{I}{U};\ \left(\frac{dP}{dU} > 0\right) \text{ left of MPP thus } U < U_{max} \tag{7}$$

$$\frac{dI}{dU} < -\frac{I}{U};\ \left(\frac{dP}{dU} < 0\right) \text{ right of MPP thus } U > U_{max} \tag{8}$$

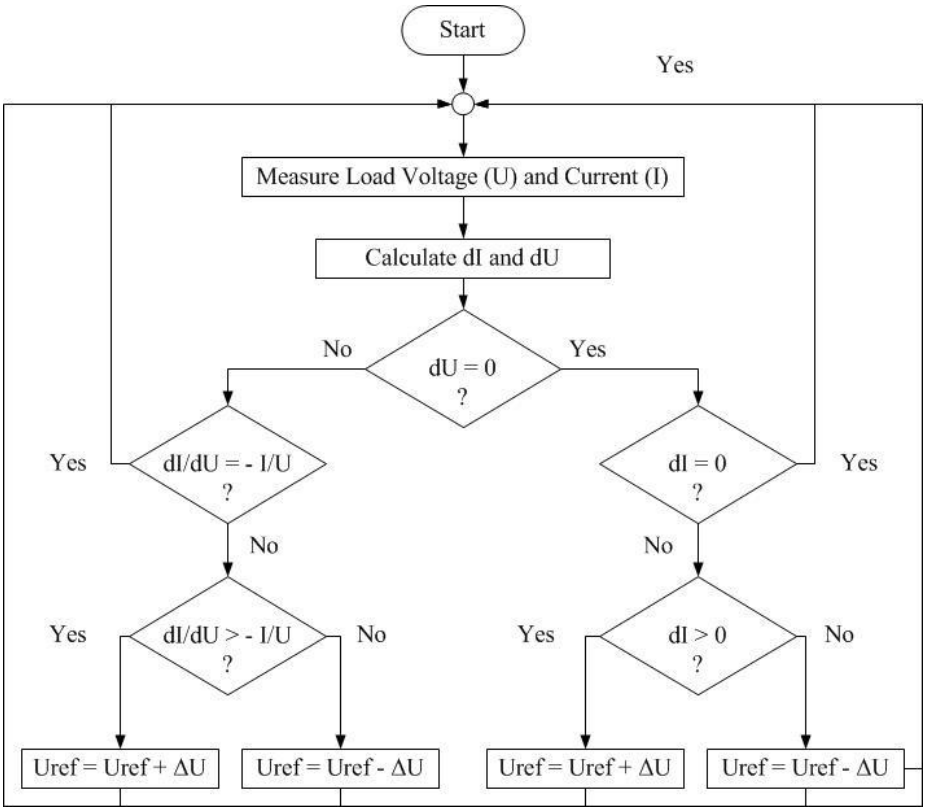

Figure 29 Flow chart of the incremental conductance method MPPT algorithm

However, this control method is complicated and the setting of adjusting voltage ΔU influences the maximum power point tracking accuracy greatly.

2.7 Conclusion

This chapter provided an overview of solar photovoltaic energy conversion system. The fundamentals of modeling solar PV cell, module and array are described. The major components of PVECS were discussed, including maximum power point tracking algorithm, DC/DC power electronic converter, DC/AC three-phase inverter, two-level VSC control system and stand-alone operation of PVECS. The results obtained from simulation are presented and discussed in this chapter. Results presented in this chapter shows the effect of varying solar irradiance, temperature, series and shunt resistances in I-V and P-V characteristics curve generated by the simulation models of solar PV cell and module. The behaviour of a stand-alone solar PVCES under variable solar irradiance is studied and results obtained from the simulation are presented in this chapter.

Chapter 3

3 Wind-Diesel Energy Conversion System

3.1 Introduction

A new technological energy solution provided by wind energy system is experiencing a high growth rate in recent days. Wind energy systems are omnipresent, freely available and environment friendly [46]. The combined wind-diesel operation is being popular all over the world since the availability of wind is unpredictable and depends on geographical and meteorological conditions. Hybrid operation increases the reliability of stand-alone system, reduces the production cost and ensures the availability of power. This type of system is often used as a potential source of electric power supply for off-grid communities and facilities [47].

This chapter demonstrates the fundamentals of wind energy conversion system (WECS), mathematical modeling of wind power extraction, electrical generator and power electronic converter interface. A maximum power point tracking method is applied to optimize the operation of wind turbine and the machine side converter controller allows access to control the speed. The modeling of diesel generator and control system for diesel energy conversion system (DECS) is explained in this chapter.

3.2 Background

Wind energy has been used for hundreds of years for milling grains, pumping water and sailing the seas. The use of windmills to generate electricity started in late nineteenth century with the development of a 12kW DC windmill generator [48]. Over the last two decades, a variety of wind power technologies have been developed, which have improved the conversion efficiency of and reduced the costs for wind energy production. The size of wind turbines has increased from few kilowatts to several megawatts each. In addition to on-land installations, large wind turbines have been pushed to offshore locations to harvest more energy and reduce their impact on land use and landscape.

Over the past few years, wind energy has shown the fastest rate of growth of any form of electricity generation with its development stimulated by concerns of national policy makers over climate change, energy diversity and security supply. In terms of transferring low-carbon energy sources, the electricity generated from wind is viewed as easier than other challenging sectors of the economy such as surface and air transport and domestic heating. Hence the use of cost-effective and reliable low-carbon electricity generation sources, in addition to demand side measures, is becoming an important objective of energy policy in many countries [45].

The availability of wind energy is very uncertain and it reduces the reliability of a power system. Although diesel generation system has many drawbacks like high maintenance, fuel supply cost, noise and hazardous gas emission issues [46], they are often integrated in such isolated system in order to provide reliability and maximize the profit [47].

A simulation model is wind-diesel conversion system is constructed to study the behaviour of a hybrid operation. The study focuses on the development and application of control systems for wind turbine and diesel generation system. This model is integrated with the solar PV system in order to develop the simulation model of stand-alone SWDHES.

3.3 Major Components of Wind Energy Conversion System

Wind energy technology has evolved rapidly over the last three decades with increasing rotor diameters and the use of sophisticated power electronics to allow operation at variable rotor speed. Major components of wind energy conversion systems are discussed below:

3.3.1 Wind Turbine

The wind turbine is one of the most important elements in wind energy conversion systems. Wind turbine produce electricity by using the power of the wind to drive an electrical generator. Wind passes over the blades, generating lift and exerting a turning force. The rotating blades turn a shaft inside the nacelle, which goes into a gearbox. The gearbox increases the rotational speed to that which is appropriate for the generator, which uses magnetic fields to convert the rotational energy into electrical energy. The power output goes to a transformer or power electronic converter, which converts the electricity from the generator by regulating the voltage.

3.3.1.1 Modeling Wind Energy Conversion System

A wind turbine extracts kinetic energy of wind through the swept area of the blades. The power in the airflow is given by [45], [44]:

$$P_{air} = \frac{1}{2}\rho A v^3 \tag{9}$$

Where, ρ is the air density, A is the swept area of rotor and v is the wind speed.

The power transferred to the wind turbine rotor is reduced by the power coefficient, C_p and it can be obtained from the following relations [45], [49]:

$$C_p = \frac{P_{wind\ turbine}}{P_{air}} \tag{10}$$

$$P_{wind\ turbine} = C_p P_{air} = P_M \tag{11}$$

The wind power captured by the blade and converted into mechanical power (P_M) can be calculated by:

$$P_{wind\ turbine} = P_M = C_p \times \frac{1}{2}\rho A v^3 \tag{12}$$

$$P_M = \frac{1}{2}\rho \pi R^2 v^3 C_p \tag{13}$$

The maximum value of C_p is defined by the Betz limit, which states that a turbine can never extract more than 59.3% of the power from an air stream [44], [50]. In reality, wind turbine rotors have maximum C_p values in the range 25-45%. It is also conventional to define a tip-speed ratio, λ, as

$$\lambda = \frac{\omega R}{v} \tag{14}$$

Where,

ω = Rotational speed of rotor

R = Radius of tip of rotor

v = Wind speed

The power coefficient, C_p of the wind turbine is a function of β and λ which is obtained from a generic expression in [51] given by equation (15).

$$C_p(\lambda, \beta) = C_1 \left(\frac{C_2}{\lambda_i} - C_3\beta - C_4\right) e^{\frac{-C_5}{\lambda_i}} + C_6\lambda \tag{15}$$

Where,

$$\frac{1}{\lambda_i} = \frac{1}{\lambda + 0.08\beta} - \frac{0.035}{\beta^3 + 1} \tag{16}$$

Equation (13) to (16) has been used in developing the mathematical model of wind turbine. The simulation model developed to generate the mechanical power produced from wind turbine is shown in fig. 30. The function and construction of MPPT block is described briefly in the section 3.4.1.

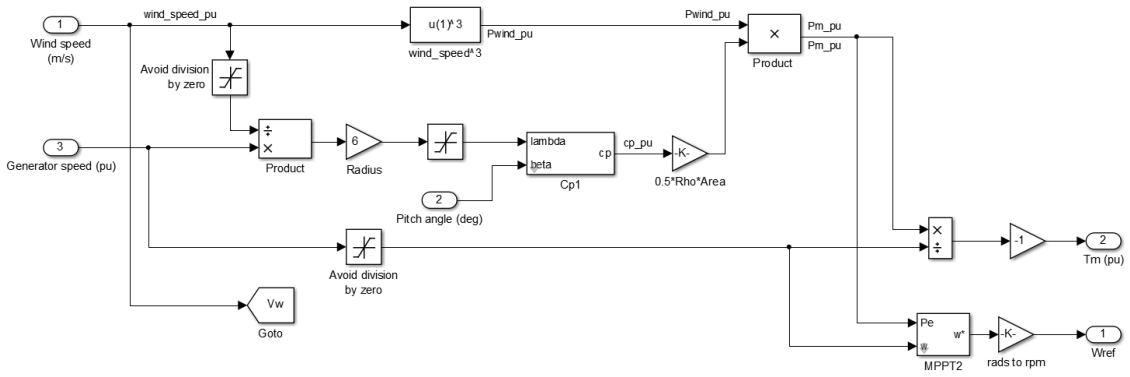

Figure 30 Subsystem of simulation model for wind power extraction

The simulation model constructed to develop WECS is given below:

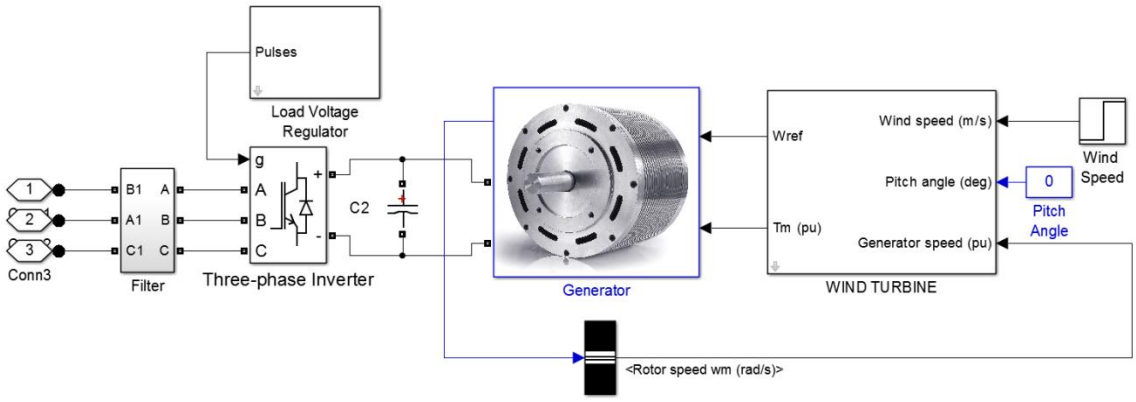

Figure 31 Subsystem of simulation model for WECS

This configuration consists of a subsystem of wind turbine model, where the mathematical model is constructed to generate the reference speed and mechanical torque as shown in fig. 30. The subsystem of the generator model consists of controllers, SimPower® block of PMSG and a machine side three-phase power electronic converter being controlled by the speed and current controllers. A load side three-phase converter is connected with the generator through a DC-link capacitor, where the converter receives PWM switching signals to regulate the load voltage. A three-phase RLC filter is

connected between the load and converter in order to improve the power quality and minimize the transition effect.

3.3.2 Electrical Generator

The evolution of wind power conversion technology has led to the development of different types of wind turbine configuration that make use of a variety of electric generators. Depending on their construction and operating principle, the wind generators are divided in two main groups: induction generators (IGs) and synchronous generators (SGs). Both induction and synchronous generators have wound rotors, which are fed by slip rings through brushes or by a brushless electromagnetic exciter.

In these days, SGs are extensively used in WECS and are classified in two types: (i) wound rotor synchronous generator (WRSG) and (ii) permanent magnet synchronous generator (PMSG). Among these two types, PMSGs are considered to be the promising option for direct driven wind turbine operation where gearboxes are not required [52]. PMSG has advantages like higher efficiency, better thermal characteristics, solid field structure, high power to weight ratio and improved dynamic stability [53]. The WECS infrastructure in TCÉ, Quebec is developed with PMSG, so the simulation is constructed according to their system configuration.

3.3.2.1 Permanent Magnet Synchronous Generator

Permanent magnet synchronous machines provide higher efficiency in lower speed applications. For given mechanical specification the use of PMSG in WECS results

smaller system size and high power density leading to maximum overall efficiency [49]. The typical construction of PMSG includes a stator and rotor. The use of permanent magnet provides brushless operation to create magnetic flux. Due to the absence of rotor windings, it is possible to achieve high power density through reduced weight and size of the machine.

The mechanical and electrical system of the machine is represented by the state space model. In order to obtain sinusoidal electromotive force, the established stator flux by permanent magnets is also chosen as sinusoidal. Due to the presence of large air gap in PMSG, it is assumed that the machine has a linear magnetic circuit and the core of either stator or rotor does not saturate. The equations for electrical and mechanical system can be obtained from the simplified *dq*-axis model of PMSG in the rotor-field synchronous reference frame [49], [54].

$$\frac{di_d}{dt} = \frac{v_d}{L_d} - \frac{Ri_d}{L_d} + \frac{L_q}{L_d} p\omega_r i_q \tag{17}$$

$$\frac{di_q}{dt} = \frac{v_q}{L_q} - \frac{Ri_q}{L_q} - \frac{L_d}{L_q} p\omega_r i_d \tag{18}$$

$$T_e = 1.5p[\varphi i_q + (L_d - L_q) i_d i_q \tag{19}$$

$$\frac{d\omega_r}{dt} = \frac{1}{J}(T_e - T_f - F\omega_r - T_m) \tag{20}$$

$$\frac{d\theta}{dt} = \omega_r \tag{21}$$

Here, equation (17) to (19) are used for electrical system where, L_d and L_q are the d and q axis inductances respectively, R is the resistance of the stator windings, i_d and i_q is the d

and q axis current respectively, v_d and v_q is the d and q axis voltage respectively, ω_r is the angular velocity of the rotor, φ is the rotor flux, p is the number of poles and T_e is the electromagnetic torque.

Mechanical equations are expressed as given in equation (20) and (21) where, J is the combined inertia of rotor and load, F is the combined viscous friction of rotor and load, θ is the rotor angular position, T_m is the mechanical torque and T_f is the shaft friction torque.

3.3.3 Power Electronic Converter Interface

Power electronic interface provides control access to the WECS through speed and torque control. A bi-directional converter unit, known as back-to-back converter, is more popular in such system. This rectifier-inverter pair is predominantly used configuration in wind energy systems, where one converter works as rectifier and other operates as inverter. Both converters work in either direction of power flow throughout the power conversion. The converter on generator side VSC is controlled using pulse width modulation (PWM) technique [45]. A DC-link capacitor is connected in between the pair in order to achieve control access. Typically the magnitude for DC-link voltage is kept higher than the load side line to line voltage [49].

The main advantage of using such configuration is, it is a well-established technology and has been applied for many years in machine drive based application. Moreover, the decoupling of VSCs through a capacitor allows separate control of the two converters [45]. The typical configuration of a back-to-back converter is like following:

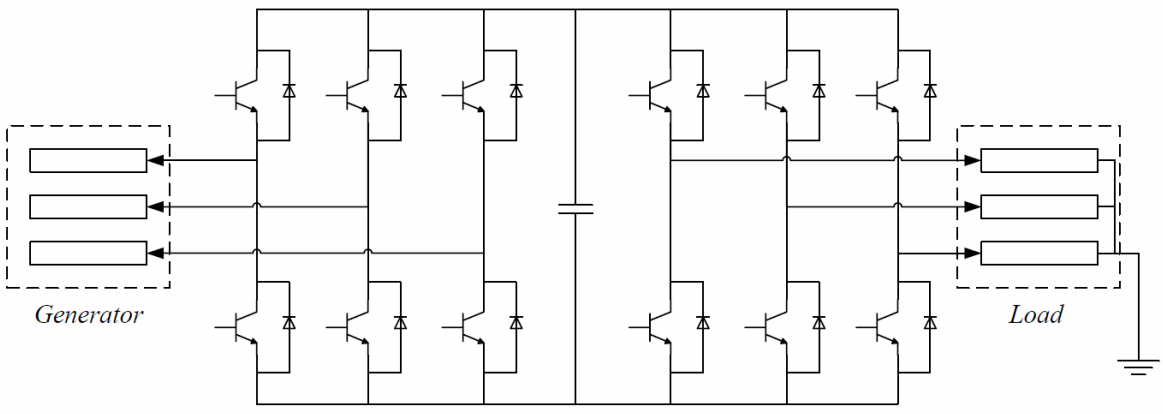

Figure 32 Back-to-back VSCs

3.4 Development of Control Systems for WECS

3.4.1 Maximum Power Point Tracking Control

The optimization of wind energy based power system mostly depends on the MPPT algorithm. Therefore, MPPT controller allows operating the wind turbine at optimum tip speed ratio to maximize the power co-efficient, by controlling the rotational speed to track the optimum speed of rotation [55]. The power coefficient, C_p depends on the tip speed ratio, λ, which depends on the turbine rotor shaft speed, ω_r. So, C_p can reach at maximum value for an optimum tip speed ratio λ_{opt}. The maximum value of C_p implies that the wind turbine converting maximum possible energy into mechanical energy [49].

In case of non-availability of wind turbine characteristics and speed, a controller is required to track the MPP by providing a reference speed. So, an improved MPPT control strategy has been developed where the wind turbine characteristics and the wind speed is not required to extract the maximum available power from wind [56]. In this algorithm, a positive gain, α, is implemented based on the power to find the speed reference, ω_{ref}, to

make the system more reliable. The power is calculated from the available wind speed using equation (13). A random parameter called speed factor, *k*, is chosen where its value changes with the variation of the turbine speed. The following expression has been developed to update the parameter in the algorithm:

$$k = \alpha\omega_r(t) \tag{22}$$

Hence, a higher value of *k* is chosen at low wind speed and with increase in wind speed the value of *k* decreases. The value of *k* is chosen (*k* = 1000) manually from simulation by trial and error method. A flowchart of the developed algorithm is shown in the fig. 33, where P_m is the mechanical power produced by the wind turbine.

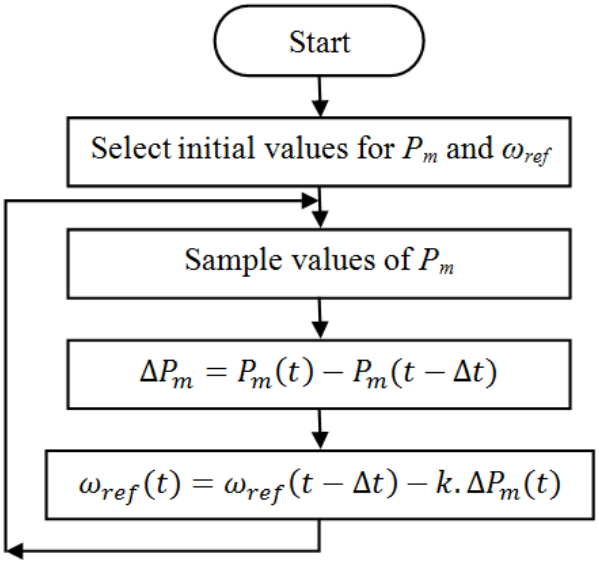

Figure 33 Flow chart of MPPT algorithm for WECS

3.4.2 Machine Side Converter Control

A control scheme based on flux weakening vector control is developed for PMSG [49]. In this system, PMSG drive consists of three-phase power converter, generator, vector controller and a speed controller. Simulation model developed for the control system is the following:

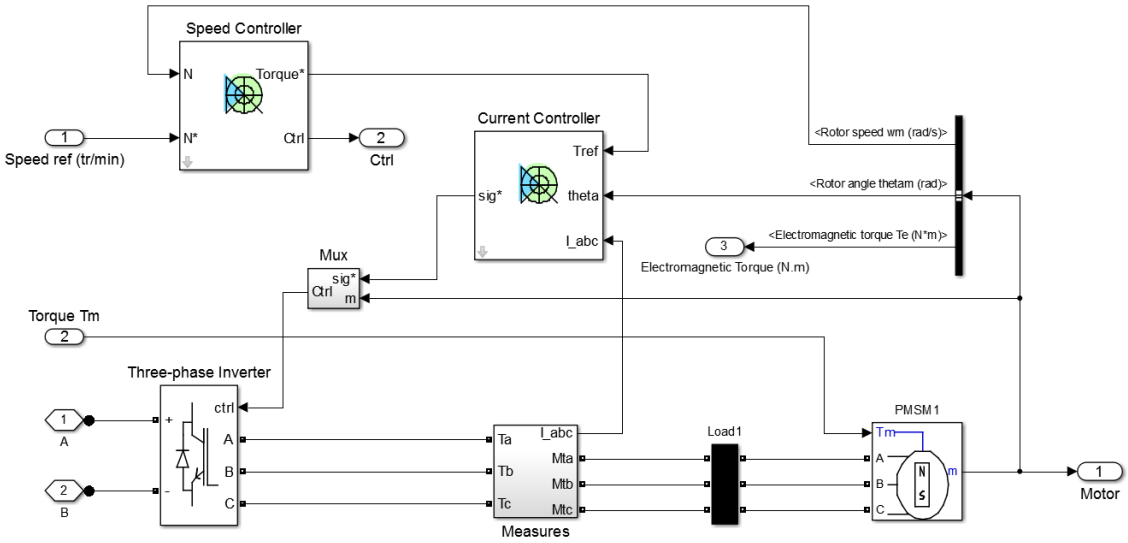

Figure 34 Subsystem of simulation model for PMSG based WECS [54]

The torque reference is obtained from the speed controller developed based on simple PI control scheme. This control scheme is obtained from [54] and constructed as shown in fig. 35.

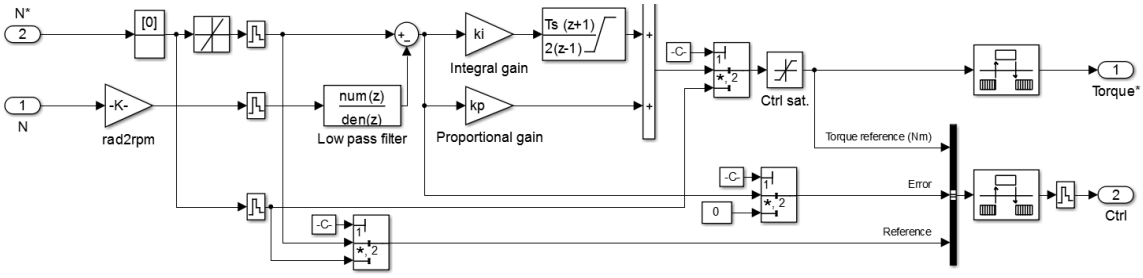

Figure 35 Simulation model of the speed controller generating torque reference [54]

The three-phase generator reference current is obtained through the vector control scheme and the controller generates PWM signals through a three-phase current regulator. This control scheme is obtained from [54] and integrated in the model shown in fig. 36.

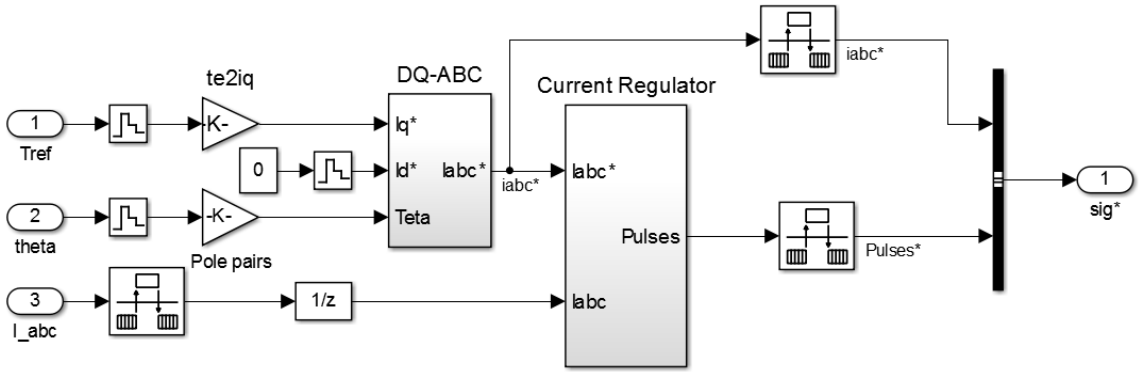

Figure 36 Simulation model of vector control scheme with current controller [54]

In order to achieve the desired torque reference, T_{ref} the nominal value of flux is maintained to regulate the line current amplitude. To achieve the desired flux weakening, the amplitude and phase of the currents are also changed in accordance with the machine torque-speed operating characteristic. The following equations are used in developing the control system, where equation (23) and (24) are used in modeling simple PI-controller

for speed control. Here, ω_{error} is the difference between the reference speed, ω_{ref} and actual rotor speed, ω_r; K_{p_torque} and K_{i_torque} is the proportional and integral gain respectively. Equation (25) and (26) are used for modeling the inputs for the current regulator, which is a simple hysteresis controller [54].

$$\omega_{error} = \omega_{ref} - \omega_r \tag{23}$$

$$T_{ref} = K_{p\_torque}(\omega_{error}) + K_{i\_torque} \int \left(\omega_{error}(t)\right) dt \tag{24}$$

$$i_q^* = \frac{2T_{ref}}{3p\varphi} \tag{25}$$

$$i_d^* = 0 \tag{26}$$

To calculate the stator reference current I_{abc}^*, the park transformation is required for I_d^*, I_q^* and electrical angle. The machine is controlled through the switching signals for power converter generated by using I_{abc}^* and three phase stator current I_{abc}.

3.5 Diesel Generator

Diesel power generators are considered as the most reliable form of emergency backup power. Because of the need of rapid response time, load carrying capacity, fuel supply, availability and reliability diesel generators are popular and effectively required in modern building code and standards. Quick response time is one of the unique features of diesel generators and it is able to absorb a full electrical load within ten seconds of power failure [57].

The typical configuration of a diesel generator consists of a diesel engine with a governor control system and a synchronous machine. The major components of a diesel engine model consists of a controller to check the steady-state error in speed and an actuator with gain *K*, time constant T_i and integrator in order to control the fuel rack position [58].

As is well known, diesel engines are highly nonlinear devices and their characteristics vary as a function of different parameters like power output, speed and ambient temperature. The existence of non-linear, time-varying, dead time between the fuel injection and production of mechanical torque, T_{mech} makes the control of diesel engine much more complex [59]. The speed of diesel engines is commonly controlled by a PI controller to prevent the steady-state error. The expression of mechanical torque, T_{mech} is obtained from the following equation where T_D is a time delay.

$$T_{mech}(s) = e^{-ST_D}\varphi(s) \tag{27}$$

The governor control system provides access to regulate the speed of the engine and in turn the power produced by controlling the diesel flow to the engine [49]. The modeling of governor control system is described briefly in section 3.6.1.

3.5.1 Synchronous Machine

A synchronous generator consists of two elements: the field and the armature [45]. The field is located on the rotor and the armature is located on the stator. The field winding carries DC electricity to produce magnetic field that rotates with the rotor shaft. This magnetic field cuts the stator conductors and three voltages while rotating. The electrical

system of a diesel generator is represented by state space model. Each phase consists of a voltage source in series with RL impedance, which represents the internal impedance of the machine. In this model, the dynamics of stator, field and damper windings are taken into consideration. The equivalent circuit in d-q rotor reference frame is shown in the figure below.

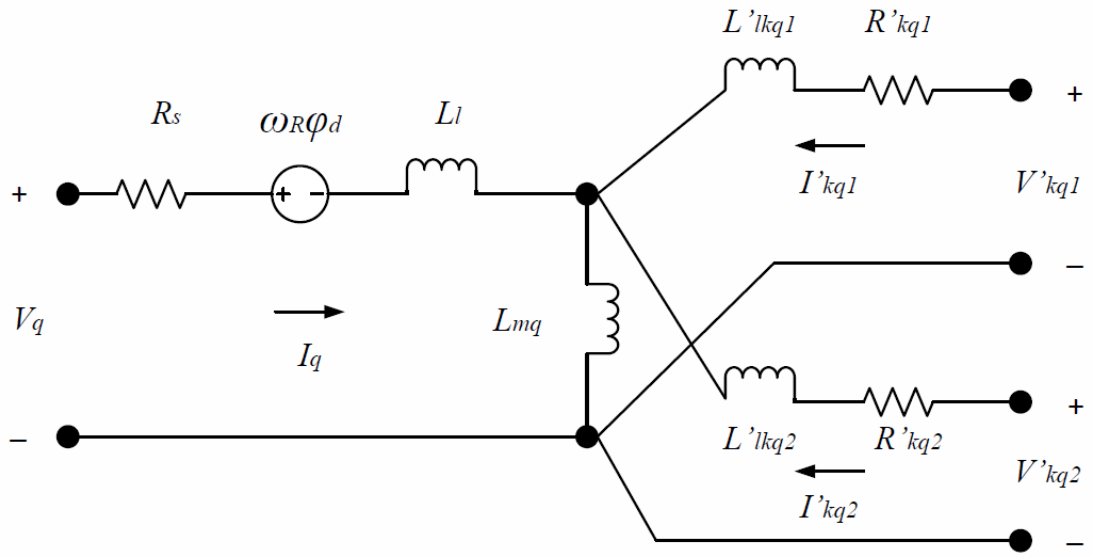

Figure 37 Equivalent circuit of electrical system of synchronous machine in q-axis frame [54]

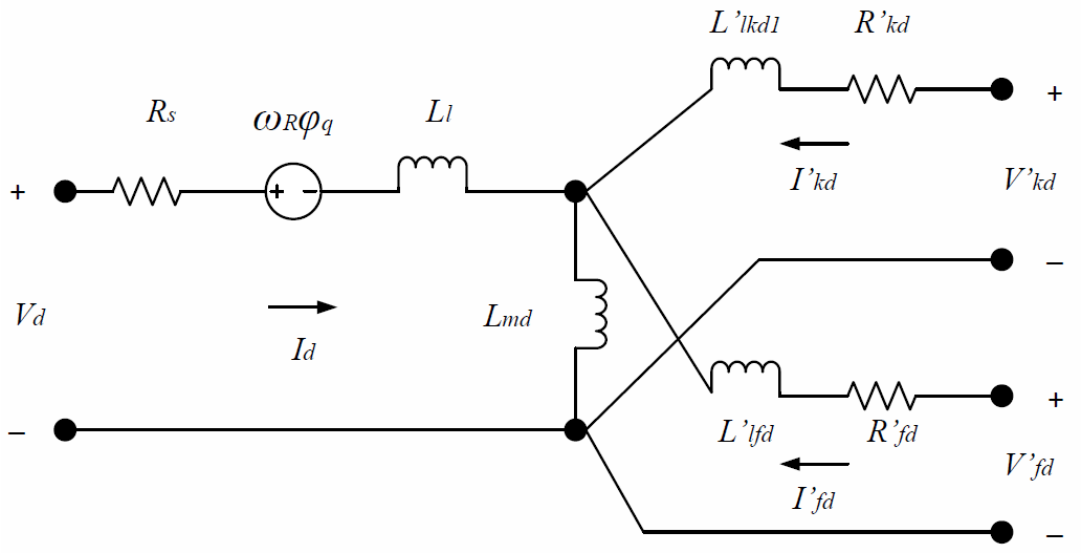

Figure 38 Equivalent circuit of electrical system of synchronous machine in d-axis frame [54]

The electrical system equations are given below [49], [54]:

$$V_d = R_s i_d + \frac{d}{dt}(\varphi_d) - \omega_R \varphi_d \tag{28}$$

$$V_q = R_s i_q + \frac{d}{dt}(\varphi_q) - \omega_R \varphi_d \tag{29}$$

$$V'_{fd} = R'_{fd} i'_{fd} + \frac{d(\varphi'_{fd})}{dt} \tag{30}$$

$$V'_{kd} = R'_{kd} i'_{kd} + \frac{d(\varphi'_{kd})}{dt} \tag{31}$$

$$V'_{kq1} = R'_{kq1} i'_{kq1} + \frac{d(\varphi'_{kq1})}{dt} \tag{32}$$

$$V'_{kq2} = R'_{kq2} i'_{kq2} + \frac{d(\varphi'_{kq2})}{dt} \tag{33}$$

Where,

$$\varphi_d = L_d i_d + L_{md}(i'_{fd} + i'_{kd}) \tag{34}$$

$$\varphi_q = L_q i_q + L_{mq} i'_{kq} \tag{35}$$

$$\varphi'_{fd} = L'_{fd} i'_{fd} + L_{md}(i_d + i'_{kd}) \tag{36}$$

$$\varphi'_{kd} = L'_{kd} i'_{kd} + L_{md}(i_d + i'_{fd}) \tag{37}$$

$$\varphi'_{kq1} = L'_{kq1} i'_{kq1} + L_{mq} i_q \tag{38}$$

$$\varphi'_{kq2} = L'_{kq2} i'_{kq2} + L_{mq} i_q \tag{39}$$

Where the subscript: a) *R*, *s* refers to the rotor and stator parameters, b) *l*, *m* refers to leakage and magnetizing inductance and c) *f*, *k* refers to field and damper winding quantity respectively.

The mechanical system equations are expressed as below [49], [54]:

$$\Delta\omega_R(t) = \frac{1}{2H}\int_0^t (T_m - T_e)dt - K_d \Delta\omega_R(t) \tag{40}$$

$$\omega_R(t) = \Delta\omega_R(t) + \omega_0 \tag{41}$$

Where, H is the inertia constant, T_m is the mechanical torque, T_e is the electromagnetic torque, K_s is the damping factor representing effect of damper windings, ω_R is the rotor speed and ω_0 is the speed of operation.

3.5.2 Excitation System

In order to supply an adjustable direct current to the main generator field winding, an excitation system is required. The exciter may be a DC generator on small set sizes. It is possible to regulate the terminal voltage when operating in generator mode [49]. The excitation system applied in this work is a DC exciter [60] and it is assumed that there is no saturation in the system.

Major components of an excitation system include a voltage regulator and an exciter circuit. The excitation system is represented by the transfer function expressed in equation (42) [54].

$$V_{fd} = \frac{E_r}{K_{ex}+sT_{ex}} \tag{42}$$

Where, V_{fd} is the exciter voltage, E_r is the output of voltage regulator, K_{ex} is the exciter gain and T_{ex} is the time constant of exciter.

3.6 Development of Control Systems for DECS

3.6.1 Governor Control System

It is possible to regulate the speed of a diesel engine by controlling the flow of diesel into the cylinders with the help of injectors. The device performs this task is known as governor in diesel generators. Regardless of any change occurring in the demand, governor is responsible to operate the engine at constant speed. In a DECS, the diesel engine acts as the prime mover which is coupled with the generator shaft in order to

generate electricity. A governor that operates the engine within a range of speed is known as the speed limiting governor [49]. A constant speed governor is chosen in this work to integrate with the hybrid system. The simulation model of the diesel engine along with a governor control system is shown in the following figure.

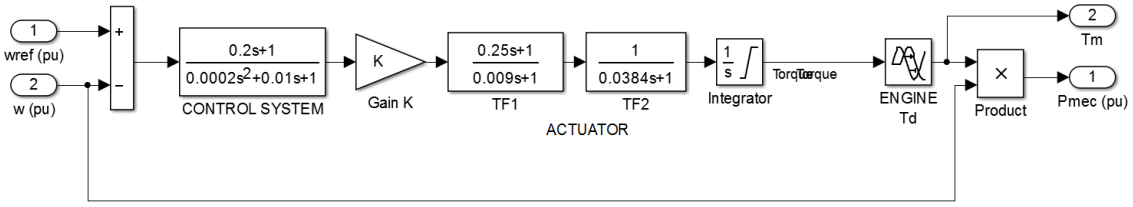

Figure 39 Model of the diesel engine with governor control system

The operating speed of a diesel generator is related to the frequency of the voltage generated as given in the below expression:

$$Generator\ frequency = \frac{Speed\ of\ the\ engine\ (in\ RPM) * Number\ of\ magnetic\ poles}{120}$$

The governor can be controlled using either speed or the frequency. But control based on speed is recommended since the generator frequency signal depends on the excitation of the generator. In case of failure in excitation, the residual magnetism may fail to generate the required signal. Such failure can damage the prime mover shaft by operating at over speed [61].

3.7 Conclusion

The construction and principle components of wind-diesel energy conversion systems are introduced in this chapter. Here, the modeling of wind turbine, PMSG based power generation, back-to-back VSC based power electronic converter interface, MPPT algorithm and the construction of machine side converter control for WECS are demonstrated. The development of SG based diesel power generation, excitation system and governor control system is described in this chapter.

Chapter 4

4 Power Management for Hybrid Systems

4.1 Introduction

The distributed power generation system based on renewable energy sources such as solar PV, wind turbines is experiencing a rapid growth around the world. Wind energy is widely being integrated in stand-alone system where solar PV systems are gaining attention [2], [8], [29]. Since the availability of wind and solar depends on geographic location and meteorological conditions, the hybrid operation of stand-alone system can improves the reliability and power quality in remote locations. Besides conventional control systems like frequency regulation and voltage regulation, a power management algorithm is required to optimize the hybrid operation

In this chapter, the method of frequency regulation and voltage regulation through a load side converter control is demonstrated. A power management algorithm is developed to share the power generated by solar PV and wind turbines where a diesel generator plays an important role in order to provide backup power and optimize the operation of SWDHES.

4.2 Frequency Regulation

Frequency regulation is a unique requirement for electrical power systems. The generated power and load demand needs to be balanced in both grid tied and stand-alone power systems. The frequency of a power system represents the stability and balance maintained between the demand and the generated power [49]. Major fluctuation may occur in the frequency of a power system due the outage of power plants or tripping of generating sources. Such problems are very common in power system operation and in order to avoid these problems a frequency regulator is required to implement in the system.

A basic frequency regulator based on dump loads is developed to regulate the frequency of stand-alone SWDHES which contains a discrete three-phase locked loop (PLL) system. Dump loads integrated in this system are variable resistive loads and are modeled using eight sets of three-phase resistors. Each set of three-phase resistor is connected in series with a gate turn-off (GTO) thyristor switches. The schematic diagram of the connection for three-phase resistive dump load and thyristors is shown in fig. 40.

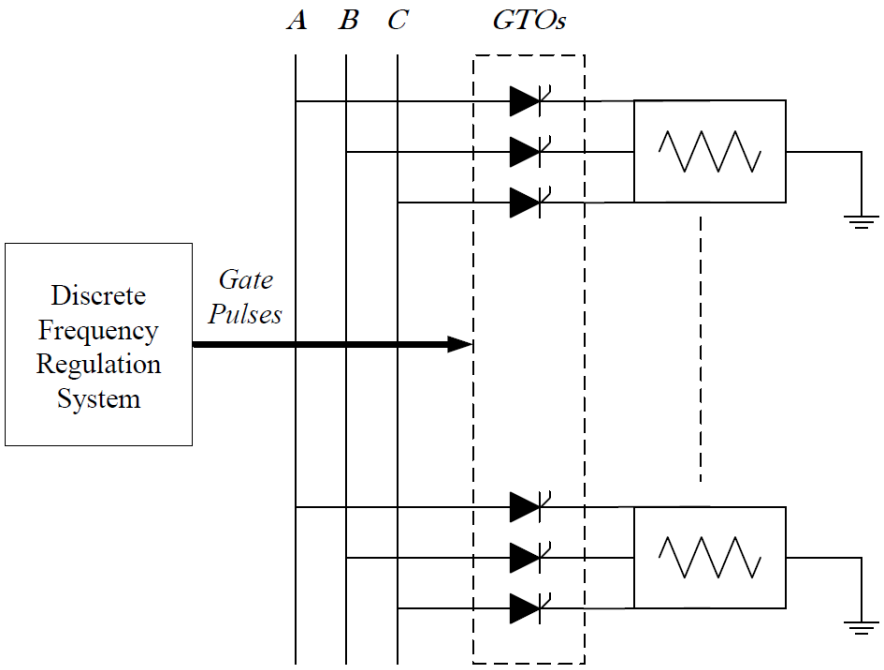

Figure 40 Schematic diagram of connection in dump load system

The power consumed by each set of three-phase resistor is 0.5 kW, these load follows a binary progression so that the dump load can be varied in ranges of values. Maximum possible power consumption by resistive dump load is 4 kW. The frequency regulation method, applied in this system, is developed for the stand-alone SWDHES configuration. In this controller, the frequency is regulated by a discrete frequency control system and a standard three-phase PLL system measures the actual frequency of the power system. The frequency error is obtained from the comparison between measured and reference frequency which is 60 Hz according to the North American Standards. A proportional-derivative (PD) controller receives the frequency error as an input to calculate the required dump load in order to regulate the system frequency. The signal from PD controller is converted to an 8-bit digital signal by passing through a sampling system.

Each bit provides switching pulse to the GTOs connected to three-phase dump loads. The switching action of these dump loads are performed at zero crossing in order to reduce fluctuations in the voltage [49]. The model of frequency regulation system is shown in fig. 41.

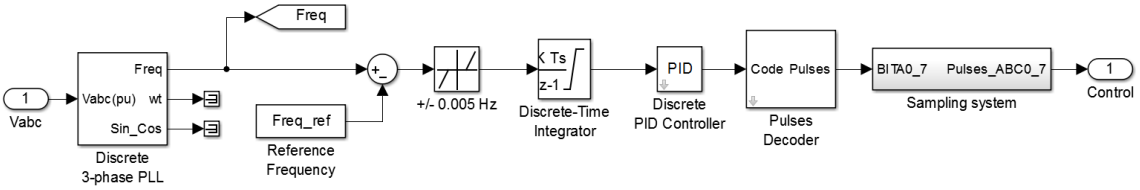

Figure 41 Model of the frequency regulation system [54]

4.3 Voltage Regulation

4.3.1 Load Side Converter Control

A voltage source converter (VSC) based controller is applied to regulate the voltage at the load side. The load side converter connected to a three-phase stand-alone utility is vector controlled in voltage reference frame. In voltage vector (d, q) reference frame the dynamic model of the converter load connection is given by [62];

$$V_d = v_{id} - Ri_d - L\frac{di_d}{dt} + \omega Li_q \tag{43}$$

$$V_q = v_{iq} - Ri_q - L\frac{di_q}{dt} - \omega Li_d \tag{44}$$

Where, *R* and *L* are the resistive and inductive components of the *RL*-filter.

The control system requires *abc* to *dq* transformation (Park's transformation) and consists of a proportional-integral (PI) controller. The output of the PI controller is again

transformed from *dq* to *abc* and afterwards 6 pulse width modulation (PWM) switching signals are generated to regulate the voltage through a three-phase inverter. Construction of the VSC control system developed for voltage regulation in hybrid power system is shown in the fig. 42.

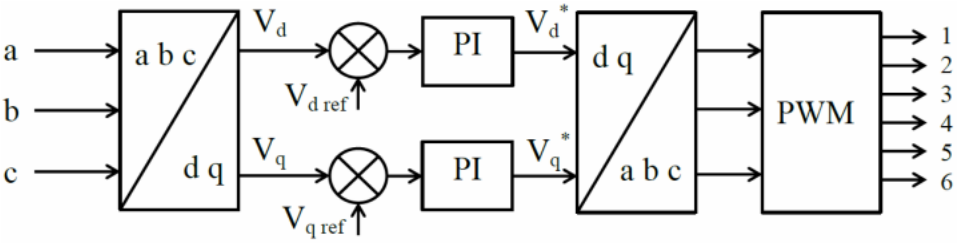

Figure 42 Schematic of the load side converter control system

A simulation model is constructed from [54] based on the equation (43) and (44) and a standard VSC control algorithm in fig. 42. The simulation model of the three-phase VSC based load side converter control system is shown in fig. 43.

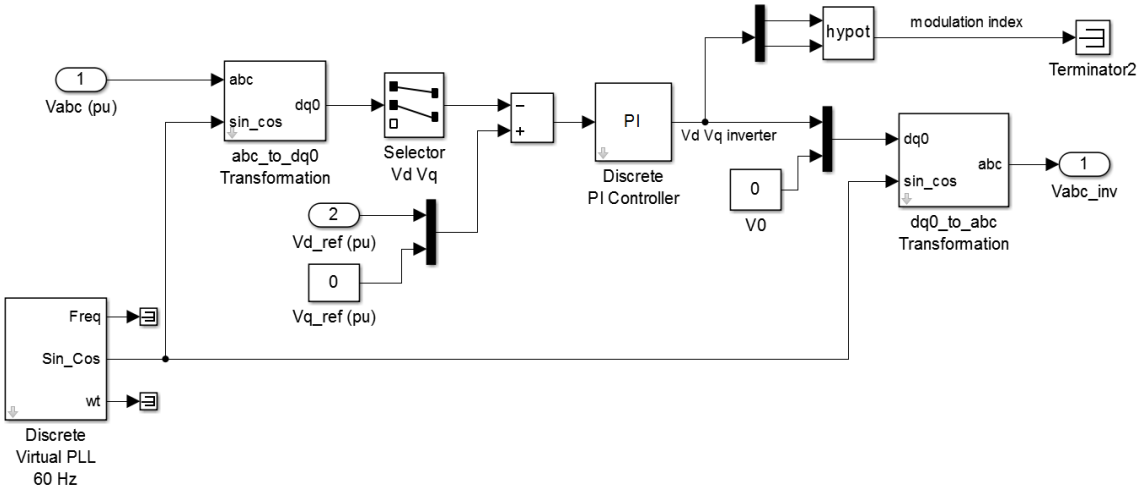

Figure 43 Simulation model of the load-side converter control system [54]

4.4 Power Management Algorithm

Compared to other renewable energy resources the availability of wind energy is very high. In this model, priority is given to wind energy since it can generate electricity both during day and night. However, solar PV is also considered to keep in operation depending on load demand. At initial stage, diesel generator provides the power supply until the power generated either from solar PV or wind energy or combined power from solar PV and wind reaches minimum 5 kW. As soon as the total generated power reaches 5 kW the supervision system turns off the diesel engine to minimize the gas emission and reduce the fuel cost.

Two sets of additional three-phase resistive loads are added depending on total generated power. If total power generation reaches 10 kW the supervision system closes the breaker for first additional load so the generated power can fed the first additional load bank. The breaker for second additional load bank is closed if the total power generation reaches 12.5 kW. So, total available load for stand-alone hybrid energy system is 15kW. The algorithm of supervision for power management is presented in the flow chart shown in fig. 44.

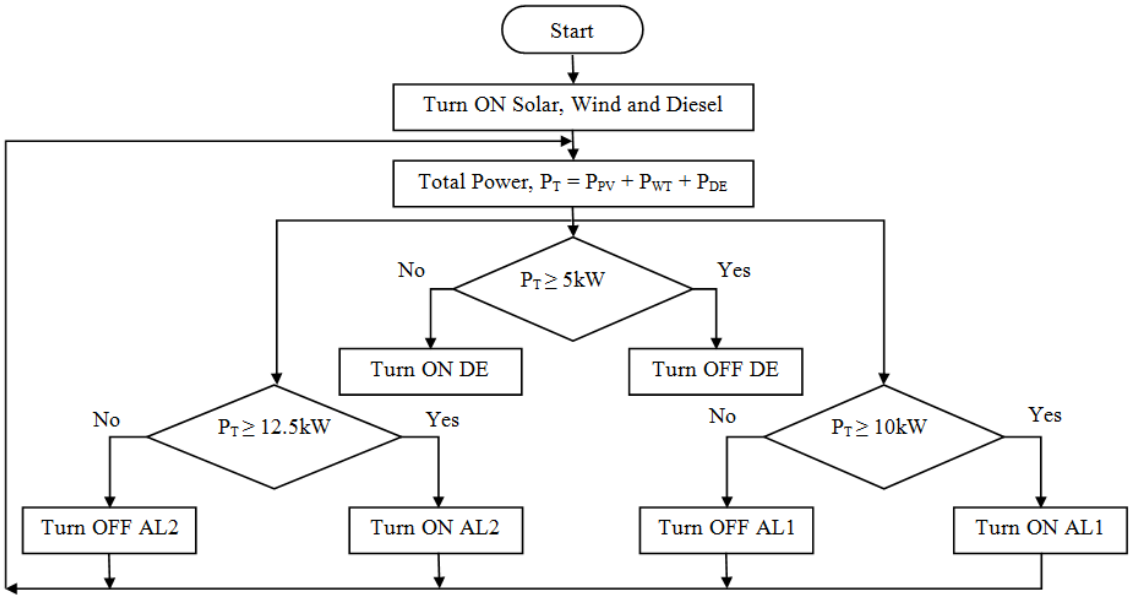

Figure 44 Flow chart of the power management algorithm for stand-alone SWDHES

Here, P_T is the total power, P_{PV}, P_{WT} and P_{DE} is the power generated by solar PV, wind turbine (WT) and diesel engine (DE) respectively. *AL1* and *AL2* are two additional resistive load banks along with the three-phase resistive main load. The simulation model constructed to integrate the power management system is shown in the fig. 45.

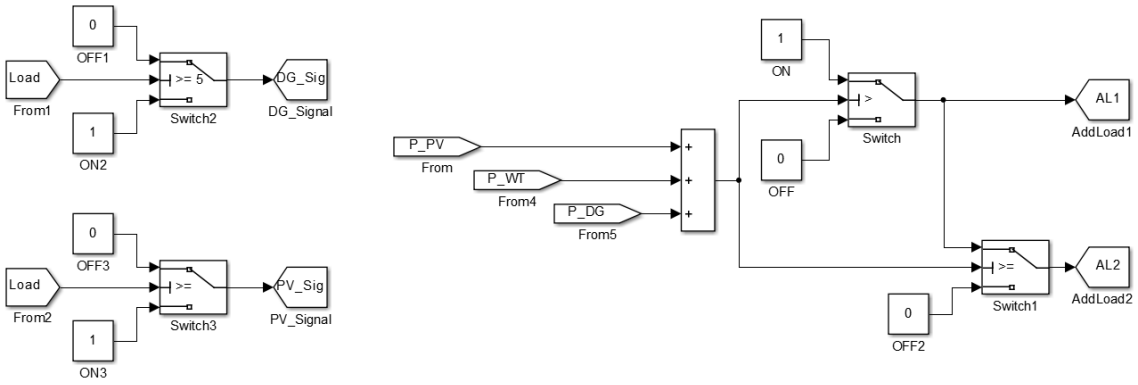

Figure 45 Simulation model of the power management algorithm

4.5 Results and Discussion

A simulation is performed to study the behavior of the power management for solar-wind-diesel stand-alone hybrid energy model. The model is constructed with Matlab®/Simulink®/SimPower® platform. The complete simulation model of SWDHES is shown in fig. 46. In this simulation block diagram, each power source and loads are connected with the bus through a controlled three-phase circuit breaker. The measurement blocks are placed between the breaker and bus for data acquisition. Power management algorithm is constructed in the SUPERVISION block and the PLOT block contains scopes to monitor the system behaviour. Control system for frequency regulation is constructed inside the FREQUENCY REGULATION block.

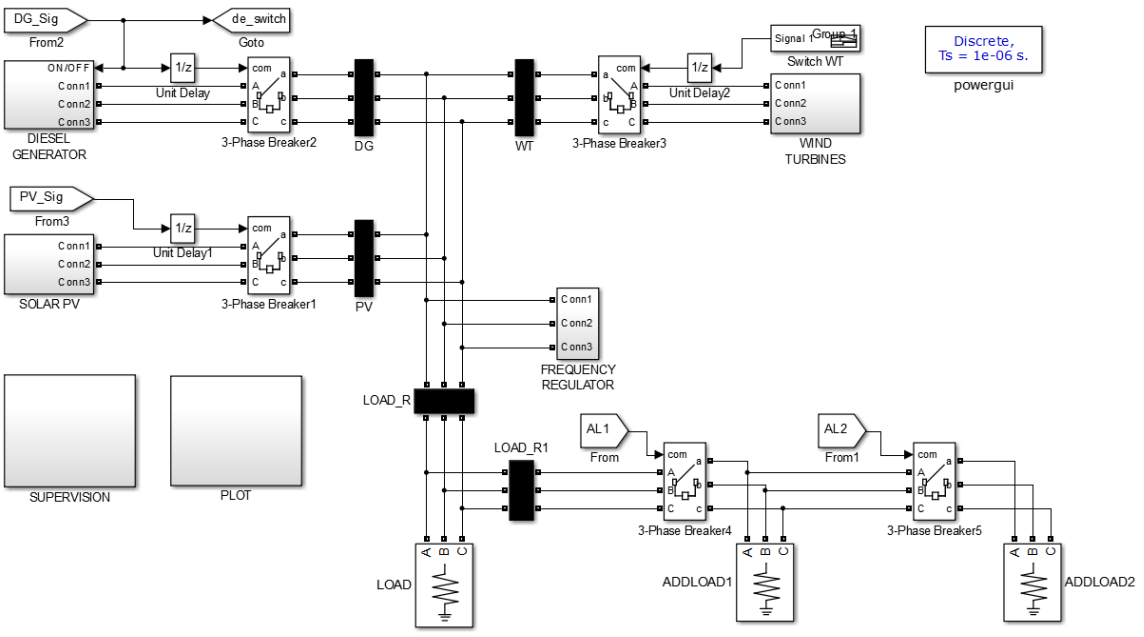

Figure 46 Simulation model of the stand-alone SWDHES

The simulation is executed in Matlab®/Simulink® simulation interface, where the Simulink® blocks of the model is processed in variable-step and SimPower® models and blocks are processed in discrete sampling. The step size for discrete sampling is $1x10^{-6}$. Results obtained from the simulation are presented in fig. 47, 48, 49, 50 and 51.

Here, fig. 47 shows the solar irradiation and wind speed profile applied in this work. A variable solar irradiance profile is applied which varies from 600 to 800 W/m^2 where the wind profile varies from 8 to 10 m/s. Fig. 48 shows the duty cycle generated by the MPPT in PVECS and reference speed generated by the MPPT in WECS. The reference speed generated by the MPPT for WECS is updated at 4.5s with the change of wind profile at 4.0 s.

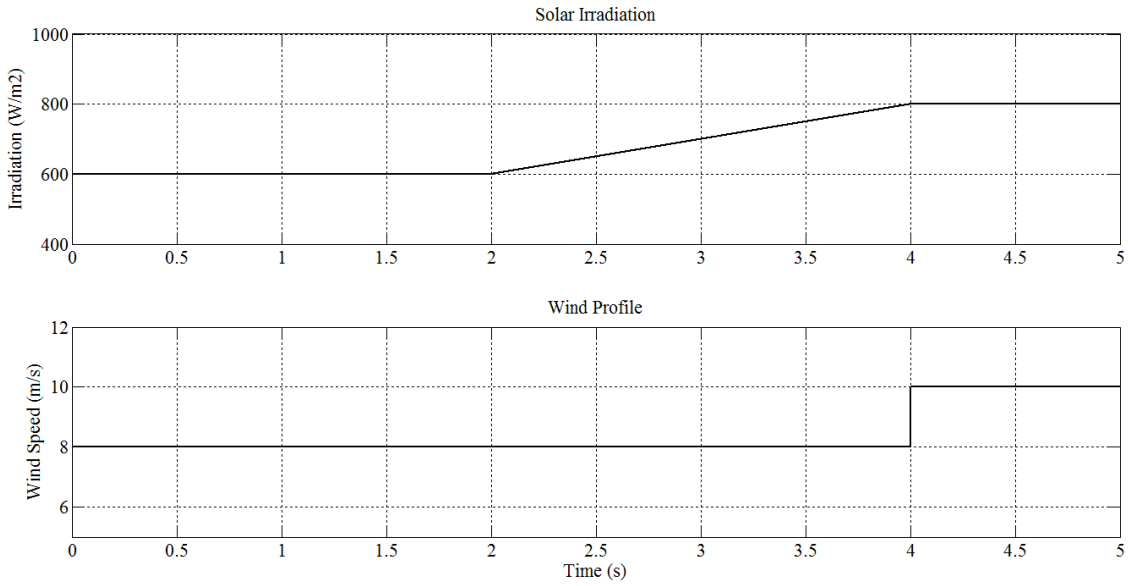

Figure 47 Variable solar irradiation and wind speed profile

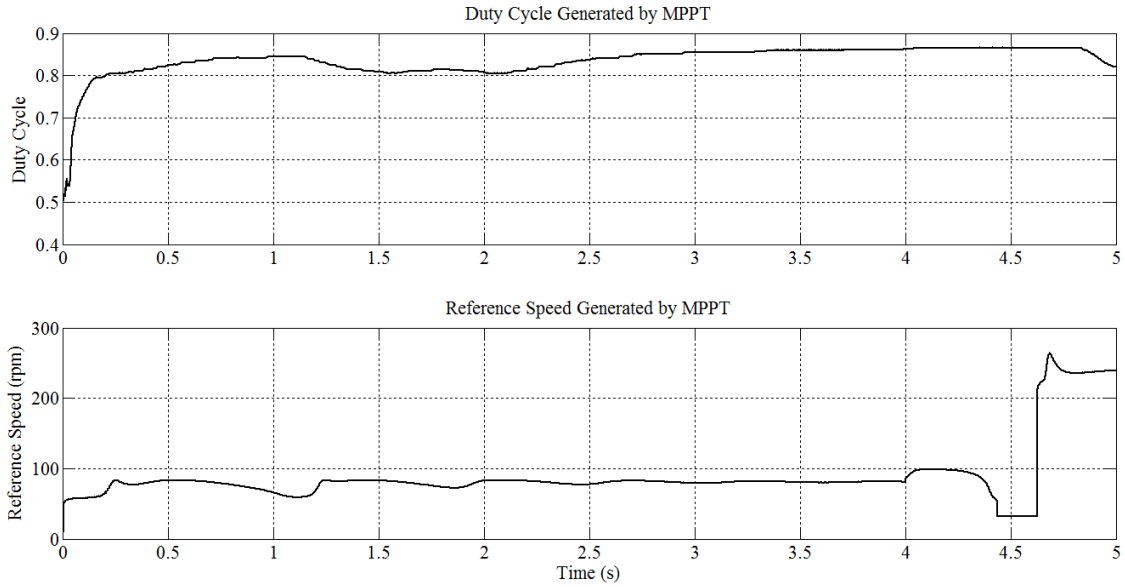

Figure 48 Duty cycle and reference speed generated by the MPPTs in PVECS and WECS respectively

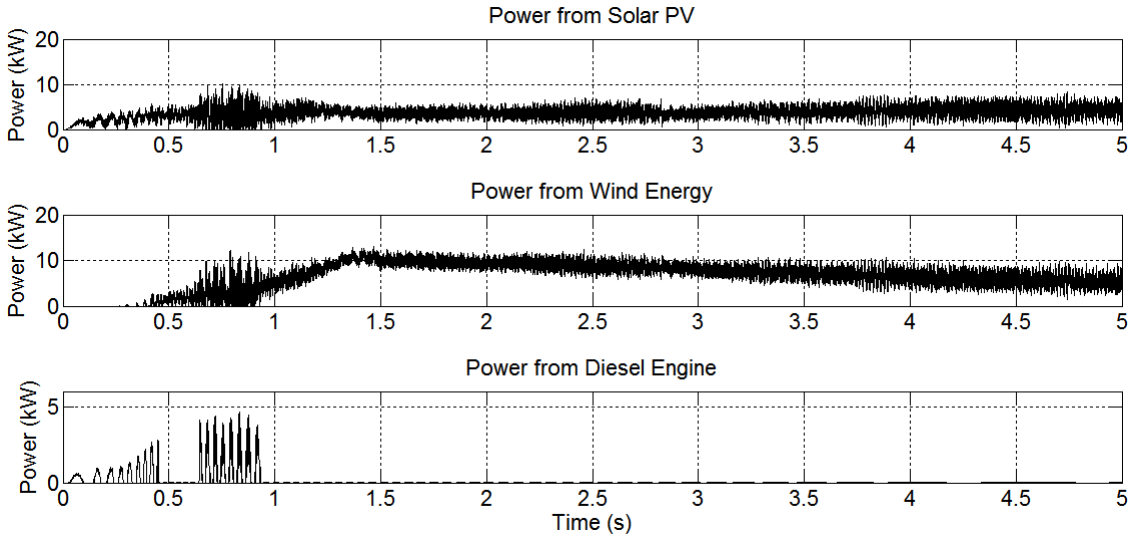

Figure 49 Power generated *(kW)* by solar PV, wind turbine and diesel generator

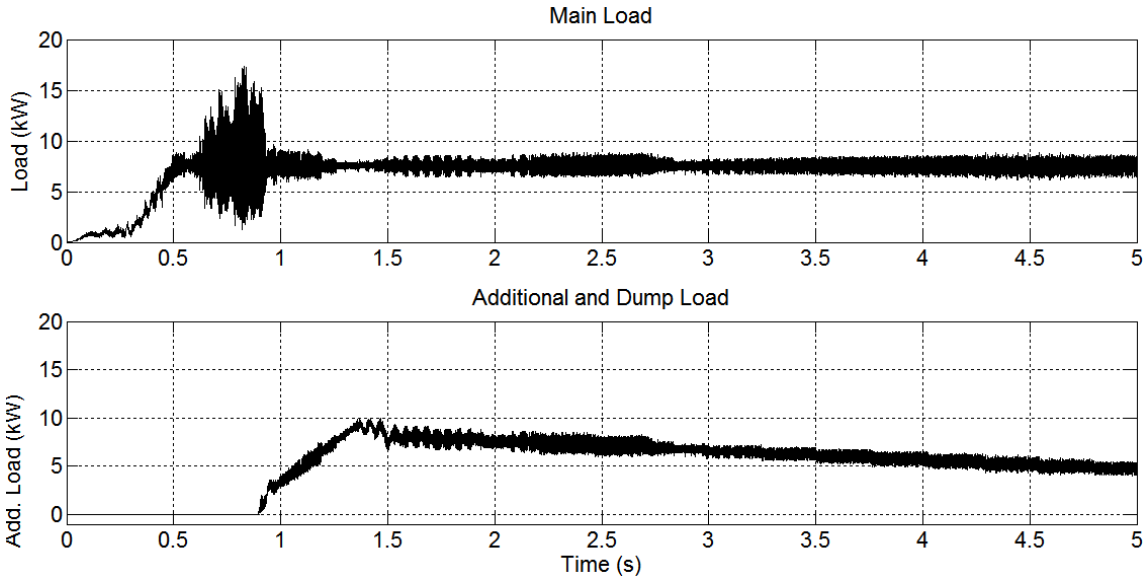

Figure 50 Total power consumption *(kW)* by main load, additional load and dump load

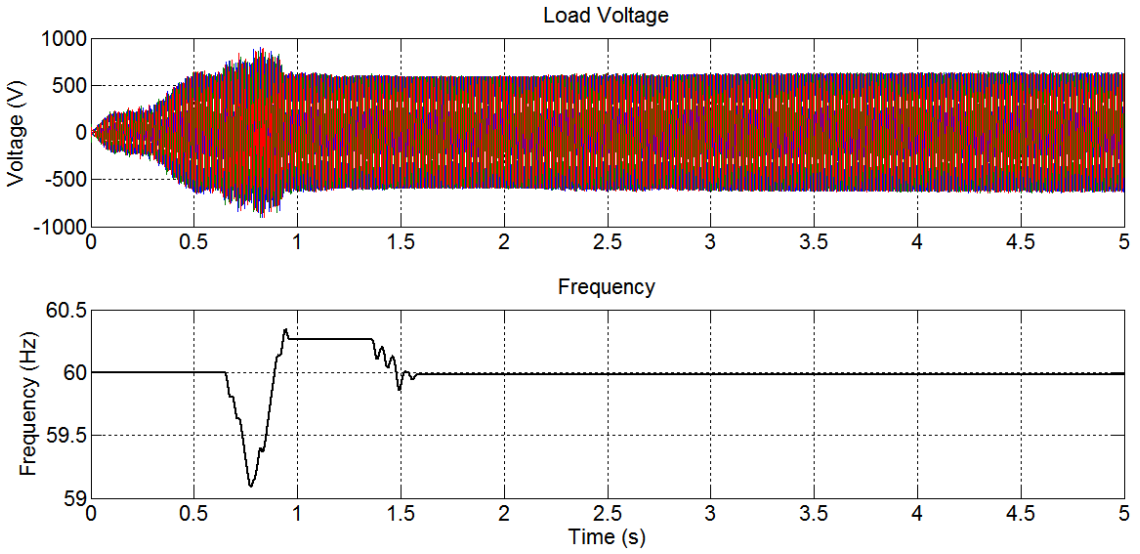

Figure 51 Status of load voltage *(V)* and frequency *(Hz)* of SWDHES

Fig. 49 Shows the power generated by solar PV, wind turbine and diesel generator. The average power generated by solar PV is approximately 6 kW. The wind turbine generates maximum 10 kW power depending on load demand. Even though, the wind speed

increases at 4.0 s the power generated by the wind turbine drops since the demand is lesser and power management algorithm turns off the dump load. Diesel engine is switched off when total generated power reaches 5 kW.

The load power consumed by the three-phase resistive main load, additional load and dump load is presented in fig. 50. The breaker for first additional load bank is closed when both solar PV and wind energy conversion system is operating and empowering 10 kW main load. Another breaker for second additional load is closed when total power generation reaches 12.5 kW.

In order to regulate the frequency, all dump loads are being added along with additional loads between 0.8 second to 1.5 second of the simulation. The frequency regulator gradually turns off the dump load one by one when the frequency is stable at 60 Hz after 1.5 second.

Since, the frequency regulator turns off the dump load when the system is stable, the power extraction from wind turbine drops due to lesser load demand. Even though, the wind speed changes to 10 m/s at 4.0 second of the simulation process, the power from wind turbine drops gradually.

Fig. 51 shows the regulation of voltage at load side and the status of system frequency. Some fluctuation in load voltage occurs between the period of 0.6 second to 0.8 second, when both solar and wind energy are added in operation. The system frequency is being affected during the same period due to same event.

4.6 Conclusion

This chapter presents an elaborative model of a SWDHES. The simulation model is developed to study the behavior of stand-alone SWDHES. A set of resistive dump load is applied to regulate the system frequency. The load side voltage is regulated with a three-phase VSC controller. A simple power management strategy is developed to improve the reliability of hybrid operation. All the results obtained from the simulation are demonstrated in this chapter.

Chapter 5

5 Conclusion and Recommendations

Hybrid energy systems (HES) can provide environment friendly and cost effective energy solutions with higher reliability and power quality. Instead of conventional energy, stand-alone solar-wind-diesel based HES can provide decent supply of electrical energy in remote locations. In these days, HES is an economic reality to reduce the dependency on a diesel fuel for off-grid communities. A diesel driven power generator is often provided in remote HES in case of unavailability of electrical power from renewable energy sources. Furthermore, HES can substantially reduce a fuel consumption and emission compared to the conventional power systems. However, a complex power management strategy is required to ensure proper power sharing between multiple sources and optimize the power quality. A brief study through simulation is focused in this research with an objective to develop a power management strategy and control systems for stand-alone solar-wind-diesel hybrid energy systems (SWDHES).

5.1 Contributions

The main contributions of this research to engineering and science are summarized below:

- A novel simulation model of stand-alone solar-wind-diesel hybrid energy system (SWDHES) was developed where a solar photovoltaic energy conversion system

(PVECS) is integrated with a wind energy conversion system (WECS) along with a diesel generator.

- A new simulation model of solar PV cell was constructed in order to develop a PV array. The power system components for PVECS are developed along with advance control techniques such as maximum power point tracking (MPPPT) to ensure maximum power extraction from PVECS.
- An advanced simulation model of PMSG based wind energy conversion system was developed and integrated into the simulation model of SWDHES along with a conventional diesel energy conversion system (DECS). An improved MPPT control scheme is developed for WECS and implemented into simulation system.
- A multi-variable control system was developed and implemented into the simulation model of SWDHES in order to operate the hybrid system at optimum level. A frequency regulator and load side voltage regulator are developed and implemented to regulate the power quality. A power management algorithm is developed and applied to optimize the hybrid operation by balancing and sharing power between sources and loads.
- The overall performance of the developed control systems and power management algorithm is validated by executing the simulation model. The results obtained from the simulation is presented and discussed in this dissertation.

TechnoCentre Éolien may apply the algorithms and control schemes developed is this research. The response of the hybrid energy system and the effect of power management

algorithm observed in this study will be useful to for hardware implementation and also for the improvement of the control algorithms in practical setup.

5.2 Recommendations for Future Work

The control system developed in this work is based on proportional-integral-derivative (PID) control and vector control scheme. However, it can be improved by applying advance control techniques like fuzzy logic control scheme, sliding mode control, adaptive control, predictive control etc. Depending on the utility size, it is possible to improve the power management system by including more conditions and complex cases. The dump load based frequency regulation system can be replaced with different form of energy storage units, such as batteries and compressed air storage system. However, grid integration of such complex system would be very challenging and further research can be conducted in this area to improve the reliability and power quality.

References

[1] H. Rudnick and A. Rudnick, "Expansion of power; facing environmental and social challenges," *IEEE Power & Energy Magazine*, pp. 14-29, 109, 17 April 2013.

[2] E. Kabalci, "Design and analysis of a hybrid renewable energy plant with solar," *Energy Conversion and Management*, vol. 72, pp. 51-59, 2013.

[3] R. Masiello and S. Venkata, "Microgrids; There may be one in your future," *IEEE Power & Energy Magazine*, pp. 14-21, 93, 19 June 2013.

[4] Government of Canada Publications, "Status of Remote/Off-Grid Communities in Canada", "Natural Resources Canada," August 2011. [Online]. Available: http://www.nrcan.gc.ca/energy/publications/sciences-technology/renewable/smart-grid/11916.

[5] "Natural Resources Canada," [Online]. Available: http://www.nrcan.gc.ca/energy/renewable-electricity/7295.

[6] European WInd Energy Association (EWEA), "Wind energy the facts: An analysis of wind energy in EU-25," 2002.

[7] "Wind Energy TechnoCentre," [Online]. Available: https://www.eolien.qc.ca/en/infrastructures-en/microgrid-wind-diesel.html.

[8] G. Bekele and B. Palm, "Feasibility study for a standalone solar–wind-based hybrid energy system for application in Ethiopia," *Applied Energy*, vol. 87, no. 2, pp. 487-495, 2010.

[9] P. Nema, R. Nema and S. Rangnekar, "A current and future state of art development of hybrid energy system using wind and PV-solar: A review," *Renewable and Sustainable Energy Reviews*, vol. 13, no. 8, pp. 2096-2103, 2009.

[10] G. Singh, "Solar power generation by PV (photovoltaic) technology: A review," *Energy*, vol. 53, pp. 1-13, 2013.

[11] L. Liu and Z. Wang, "The development and application practice of wind–solar energy hybrid generation systems in China," *Renewable and Sustainable Energy*

Reviews, vol. 13, no. 6, pp. 1504-1512, 2009.

[12] W. Zhou, C. Lou, Z. Li, L. Lu and H. Yang, "Current status of research on optimum sizing of stand-alone hybrid solar–wind power generation systems," *Applied Energy,* vol. 87, no. 2, pp. 380-389, 2010.

[13] V. Rajasekaran, A. Merabet and H. Ibrahim, "Modeling, Simulation and Development of Supervision/Control System for Hybrid Wind Diesel System Supplying an Isolated Load," 2012.

[14] H. Li and Z. Chen, "Design optimization and site matching of direct-drive permanent magnet wind power generator systems," *Renewable Energy,* vol. 34, no. 4, pp. 1175-1184, 2009.

[15] S. Liu, S. Li and L. He, "Direct-driven permanent magnet synchronous wind-power generating system with two three-level converters based on SVPWM control," *Procedia Engineering,* vol. 29, pp. 1191-1195, 2012.

[16] J. Thongam, R. Beguenane, M. Tarbouchi, A. Okou, A. Merabet, I. Fofana and P. Bouchard, "A rotor speed estimation algorithm in variable speed permanent magnet synchronous generator wind energy conversion system," *International Journal of Robust and Nonlinear Control,* vol. 23, no. 16, pp. 1880-1890, 2013.

[17] C. Jauch, S. Islam, P. Sorensen and B. Jensen, "Design of a wind turbine pitch angle controller for power system stabilization," *Renewable Energy,* vol. 32, no. 14, pp. 2334-2349, 2007.

[18] H. Camblong, "Digital robust control of a variable speed pitch regulated wind turbine for above rated wind speeds," *Control Engineering Practice,* vol. 16, no. 8, pp. 946-958, 2008.

[19] A. Merabet, R. Beguenane, J. Thongam and H. Ibrahim, "Adaptive sliding mode speed control for wind turbine systems," *IECON 2011-37th Annual Conference on IEEE Industrial Electronics Society,* pp. 2461-2466, 2011.

[20] M. Green, Power to the people: sunlight to electricity using solar cells, UNSW Press, 2000.

[21] M. Molina and E. Espejo, "Modeling and simulation of grid-connected photovoltaic energy conversion systems," *International Journal of Hydrogen Energyq,* vol. 39,

pp. 8702-8707, 2014.

[22] S. Kebaili and A. Betka, "Design and Simulation of Stand Alone Photovoltaic Systems," *WSEAS Transactions on Power Systems,* vol. 6, no. 4, pp. 89-99, 2011.

[23] D. Hohm and M. Ropp, "Comparative study of maximum power point tracking algorithms," *Progress in photovoltaics: Research and applications,* vol. 11, no. 1, pp. 47-62, 2003.

[24] L. Qin and X. Lu, "Matlab/Simulink-based research on maximum power point tracking of photovoltaic generation," *Physics Procedia,* vol. 24, pp. 10-18, 2012.

[25] C. Chiu, Y. Ouyang and C. Ku, "Terminal sliding mode control for maximum power point tracking of photovoltaic power generation systems," *Solar Energy,* vol. 86, no. 10, pp. 2986-2995, 2012.

[26] H. Yang, L. Lu and W. Zhou, "A novel optimization sizing model for hybrid solar-wind power generation system," *Solar Energy,* vol. 81, no. 1, pp. 76-84, 2007.

[27] M. Ambia, M. Islam, M. Shoeb, M. Maruf and A. Mohsin, "An analysis & design on micro generation of a domestic solar-wind hybrid energy system for rural & remote areas-perspective Bangladesh," *2010 2nd International Conference on Mechanical and Electronics Engineering (ICMEE),* vol. 2, pp. 107-110, 2010.

[28] R. Li, B. Wu, X. Li, F. Zhou and Y. Li, "Design of wind-solar and pumped-storage hybrid power supply system," *2010 3rd IEEE International Conference on Computer Science and Information Technology (ICCSIT),* vol. 5, pp. 402-405, 2010.

[29] Y. Huang, Y. Xu and X. Zhou, "Study on wind-solar hybrid generating system control strategy," *2011 International Conference on Multimedia Technology (ICMT),* pp. 773-776, 2011.

[30] C. Jian, C. Yanbo and Z. Lihua, "Design and research of off-grid wind-solar hybrid power generation systems," *2011 4th International Conference on Power Electronics Systems and Applications (PESA),* pp. 1-5, 2011.

[31] Y. Jiang, J. Qahouq and I. Batarseh, "Improved solar PV cell Matlab simulation model and comparison," *Proceedings of 2010 IEEE International Symposium on Circuits and Systems (ISCAS),* pp. 2770-2773, 2010.

[32] T. Salmi, M. Bouzguenda, A. Gastli and A. Masmoudi, "Evaluating solar photovoltaic system performance using MATLAB," *2012 First International Conference on Renewable Energies and Vehicular Technology (REVET),* pp. 55-59, 2012.

[33] B. Manju, R. Ramaprabha and B. Mathur, "Modelling and control of standalone solar photovoltaic charging system," *2011 International Conference on Emerging Trends in Electrical and Computer Technology (ICETECT),* pp. 78-81, 2011.

[34] Canadian Solar, "Canadian Solar CS6P 240/245/250/255/260M Datasheet," 2013. [Online]. Available: http://www.canadiansolar.com/.

[35] W. Xiao, F. Edwin, G. Spagnuolo and J. Jatskevich, "Efficient approaches for modeling and simulating photovoltaic power systems," *IEEE Journal of Photovoltaics,* vol. 3, no. 1, pp. 500-508, 2013.

[36] W. Shen, Y. Ding, F. Choo, P. Wang, P. Loh and K. Tan, "Mathematical model of a solar module for energy yield simulation in photovoltaic systems," *International Conference on Power Electronics and Drive Systems,* pp. 336-341, 2009.

[37] M. Vitorino, L. Hartmann, A. Lima and M. Corrêa, "Using the model of the solar cell for determining the maximum power point of photovoltaic systems," *European Conference on Power Electronics and Applications,,* pp. 1-10, 2007.

[38] W. Chen, H. Shen, B. Shu, H. Qin and T. Deng, "Evaluation of performance of MPPT devices in PV systems with storage batteries," *Renewable Energy,* vol. 32, no. 9, pp. 1611-1622, 2007.

[39] M. Islam, A. Merabet, R. Beguenane and H. Ibrahim, "Modeling solar photovoltaic cell and simulated performance analysis of a 250W PV module," *2013 IEEE Electrical Power & Energy Conference (EPEC),* pp. 1-6, 2013.

[40] E. Banu and M. Istrate, "Modeling and simulation of photovoltaic arrays," *Buletinul AGIR,* vol. 3, pp. 161-166, 2012.

[41] S. Said, A. Massoud, M. Benammar and S. Ahmed, "A Matlab/Simulink based photovoltaic array model employing SimPowerSystems toolbox," *Journal of Energy and Power Engineering,* vol. 6, pp. 1965-1975, 2012.

[42] T. Bennett, A. Zilouchian and R. Messenger, "Photovoltaic model and converter

topology considerations for MPPT purposes," *Solar Energy*, vol. 86, no. 7, pp. 2029-2040, 2012.

[43] M. Islam, A. Merabet, R. Beguenane and H. Ibrahim, "Simulation based study of maximum power point tracking and frequency regulation for stand-alone solar photovoltaic systems," *Renewable Energy and Power Quality Journal*, vol. 12, pp. 1-5, 2014.

[44] B. Wu, Y. Lang, N. Zargari and S. Kouro, Power conversion and control of wind energy systems, John Wiley & Sons, 2011.

[45] O. Anaya-Lara, N. Jenkins, J. Ekanayake, P. Cartwright and M. Hughes, Wind energy generation: modeling and control, John Wiley & Sons, 2011.

[46] A. Kaabeche and R. Ibtiouen, "Techno-economic optimization of hybrid photovoltaic/wind/diesel/battery generation in a stand-alone power system," *Solar Energy*, vol. 103, pp. 171-182, 2014.

[47] Y. Hu and P. Solana, "Optimization of a hybrid diesel-wind generation plant with operational options," *Renewable Energy*, vol. 51, pp. 364-372, 2013.

[48] T. Burton, N. Jenkins, D. Sharpe and E. Bossanyi, Wind energy handbook, John Wiley & Sons, 2011.

[49] V. Rajasekaran, "Modeling, simulation and developement of supervision control system for hybrid wind diesel system," Saint Mary's University, 2013.

[50] G. Abad, J. Lopez, M. Rodriguez, L. Marryoyo and G. Iwanski, Double fed induction machine: modeling and control for wind energy generation, John Wiley & Sons, 2011.

[51] H. Siegfried, Grid integration of wind energy conversion systems, John Wiley & Sons Ltd, 1998.

[52] G. Pellegrino, P. Torino, F. Villata, P. Guglielmi and A. Vagati, "Design of direct-driven, low-speed PM machines," in *Industry Applications Conference*, 2003.

[53] P. Sharma, W. Sulkowski and B. Hoff, "Dynamic stability study of an isolated wind-diesel hybrid power system with wind power generation using IG, PMIG and PMSG: A comparison," *International Journal of Electrical Power & Energy*

Systems, vol. 53, pp. 857-866, 2013.

[54] MathWorks Inc., "Mathworks Documentation Center, Simpower Systems," 2014. [Online]. Available: http://www.mathworks.com/help/physmod/sps/motors-and-generators.html.

[55] A. Merabet, M. Islam, R. Beguenane and H. Ibrahim, "Second-order sliding mode control for variable speed wind turbine experiment system," *Renewable Energy and Power Quality Journal,* vol. 12, pp. 1-5, 2014.

[56] A. Merabet, M. Islam and R. Beguenane, "Predictive speed controller for laboratory size wind turbine experiment system," *2014 Canadian Conference on Electrical and Computer Engineering,* pp. 1-6, 2014.

[57] "Diesel Technology Forum," [Online]. Available: http://www.dieselforum.org/files/dmfile/DTF_powergen_2013factsheet_FIN1.pdf.

[58] L. Hannett, F. De Mlello, G. Tylinski and W. Becker, "Validation of nuclear plant auxiliary power supply by test," *Power Apparatus and Systems, IEEE Transactions on,* vol. 9, pp. 3068-3074, 1982.

[59] S. Roy, O. Malik and G. Hope, "An adaptive control scheme for speed control of diesel driven power-plants," *Energy Conversion, IEEE Transactions on,* vol. 6, no. 4, pp. 605-611, 1991.

[60] *IEEE Recommended practices for excitation system models for power system stability studies,* New York: IEEE Power Engineering Society, 2005.

[61] A. David, "Generator basics applied to field problems," in *NETA World Magazine,* 1993.

[62] A. Merabet and J. Thongam, "Predictive tracking controller for induction generator in variable speed wind energy conversion systems," *Electric Power and Energy Conference (EPEC), 2010 IEEE,* pp. 1-6, 2010.

Appendix A

Specifications of the Systems Developed in Simulation Study

A. Specifications of Solar PVECS

Variable irradiation = 600 to 800 W/m^2

Optimum operating voltage of PV modules = 30.4 V

Optimum operating current of PV module = 8.22 A

Nominal power generated by each module = 250 W

Optimum operating voltage of PVarray = 121.6 V

Optimum operating current of PV array = 49.32 A

Nominal power generated by PVECS = 6 kW

B. Specifications of PMSG based WECS

c_1 = 0.517, c_2 = 116, c_3 = 0.4, c_4 = 5, c_5 = 21 and c_6 = 0.0068

ρ = 1.225 kg/m^3

Rotor diameter = 82.5 m

Rotor swept area = 107.5 m^2

Nominal power generated by wind turbine = 30 kW

C. Specifications of DECS

R_S = 0.0036 pu

H = 1.07 pu

Pole pairs = 2

Nominal power = 52.5 kW

D. Specification of Stand-alone System

Operating three-phase RMS voltage (phase to phase) = 600 V

System frequency = 60 Hz

Main load = 10 kW

Additional load 1 = 2.5 kW

Additional load 2 = 2.5 kW

Dump load = 4 kW